AN INVESTIGATION OF THE EJECTOR-POWERED JET-FLAP

Thesis by

Laurent B. Sidor

In Partial Fulfillment of the Requirements

For the Degree of

Aeronautical Engineer

California Institute of Technology

Pasadena, California

1974

(Submitted September 10, 1973)

ACKNOWLEDGEMENTS

The author expresses his gratitude to Dr. Gordon L. Harris for suggesting the topic and providing guidance in the early part of the work. Also, he is grateful to Dr. Homer J. Stewart for his interest and his guidance in the completion of this work. In addition, the financial support of the National Aeronautics and Space Administration, Ames Research Center is deeply appreciated. And finally, he thanks Mrs. Elizabeth Fox for the typing of the thesis.

ABSTRACT

The inviscid and incompressible potential flow aspects associated with a two-dimensional ejector-powered jet-flap configuration are investigated. The energy addition due to the mixing process in the ejector results in a non-homogeneous flow and is represented by an actuator disk located between the lifting surfaces and a powered wake. A set of singularities is developed to represent the lifting surfaces, to include camber and flap deflection, and the powered wake. A numerical procedure is used to compute the total system vorticity needed to satisfy exactly all the prescribed boundary conditions. The lift and moment coefficients are evaluated as a function of the head change prescribed across the actuator disk. A simple interpretation of the resulting lift curves is proposed in terms of analytical results obtained for single-airfoil configurations - a flat-plate airfoil and sink system, and a conventional single element jet flap. The sink effect of the actuator accounts for a finite lift at zero angle of attack, and the lift increment due to angle of attack only can be predicted by using Spence's theory of the jet flap.

TABLE OF CONTENTS

TABLE OF CONTENTS (Cont'd)

TABLE OF CONTENTS (Cont'd)

I. INTRODUCTION

1. General Background

The past few years have seen a widened interest in the area of V/STOL flight, spurred by potentially attractive civilian and military applications. These applications establish as a foremost requirement for the lifting system a high wing loading, necessary for range and good ride quality.

Toward the satisfaction of this requirement, new aerodynamic configurations have been developed to exploit directly the power available from the propulsion system for the generation of lift by blowing on the lifting surfaces. Various schemes have been investigated, and are shown in Fig. 1. They are:

The externally blown flap (a good review of configurations of this type is in Ref. 29) and over the wing blowing (Ref. 28) configurations use the jet engine exhaust directly over the upper side of the flap or wing surface. These configurations are characterized by the simplicity of the mechanical devices used to direct the exhaust airflow.

Other configurations use an extensive internal ducting system, driven by the high pressure stage of the engine compressor, to distribute the blowing over a major spanwise portion of the wing. The conventional jet-flap (Refs. 30-31) and augmentor-type wings operate on this principle.

In a conventional jet-flap, the jet sheet created by the blowing action mixes with the surrounding air producing a secondary effect on the lift by fact rather than design; it will be discussed later in this

section. On the other hand, the name "augmentor wings" is reserved for configurations intended to exploit this mixing effect to "augment" the primary airstream with the entrained secondary in installations known as "ejectors." The specific purpose for which the ejector is designed separates augmentor wings into two categories.

(a) The ejector can develop extra thrust on its inlet lip and sidewalls, thus supplementing the direct thrust generated by the primary for a vertical lift system.

A family of ejectors designed toward this end has been under development at the Aerospace Research Laboratories, Wright Patterson AFB (Refs. 19, 20). It is specifically tailored for the needs of vertical take-off and landing operations.

(b) The other type of augmentor wing is the ejector-powered jet-flap, which is the subject of the present investigation. The purpose of the ejector in this case is to augment the primary jet momentum with the entrained secondary, the intent being to produce an increase in circulation around the wing as compared to a conventional jet-flap design, other things being equal. In addition, the design is purported to offer a potential remedy to the noise problem associated with conventional jet-flaps. The ejector-powered jet-flap is aimed at producing the high lift coefficients needed for sustaining flight at low forward speeds: this is the domain of STOL. The Large-Scale Aerodynamics facility at NASA/Ames has tested several full-scale versions of this scheme (Refs. 26, 27).

The present work is concerned with the analysis of some aspects of the flow field around a two-dimensional section of this

type. Let us describe now in more specific terms the flow field and how the conventional modelling techniques can be extended to the present problem.

2. Representation of the Effects of the Mixing Zone on the Lifting Surfaces

The effects of the mixing zone are represented by the inflow velocity associated with the jet entrainment, and a net momentum flow downstream resulting in a powered wake. The inflow velocity can in turn be represented as an equivalent distribution of sinks located on the jet centerline (Ref. 33), the strength of these sinks being equal to the rate of entrainment. The net momentum flux in the powered wake is representative of the mixing efficiency of the ejector. The specific parameters used depend on the wake model used and are discussed in the next section.

3. Solutions to the Lifting Problem for Multi-energy Flows

A wide variety of multi-energy potential flows have been investigated over the past fifteen years or so, and are quite intimately associated to new developments in lifting systems. The flow models can be classified into two families: thin wake models and thick wake models. The independent parameter used to describe the energy addition will depend on which wake model is used.

Spence, in his analysis of jet-flap configurations (Refs. 5, 6, 13), used a thin wake model, in which the real powered wake is replaced by a single vortex sheet. In addition the boundary conditions are linearized. This model is valid in the limit of a jet of negligibly small mass flux but finite momentum flux (it is the independent

parameter energy addition due to the jet).

His analysis was extended by Wygnanski and Newman (Ref. 7) to include the effects of entrainment by adding sinks on the airfoil chordline. The strength of the sinks, for a given jet momentum, is related to the entrainment as mentioned previously. It is found that although significant, the contribution of the sinks to the over-all lift increment is quite small, and possibly dependent on the particular mixing model used.

Thick wake work has been largely associated with the prediction of propeller configurations, with the exception of C. A. Shollenberger's investigation of the two-dimensional propulsive biplane (Ref. 8). The independent parameter, in this case, is the head change ΔH normalized in the form $C_H = \frac{\Delta H}{\frac{1}{2}\rho U_\infty^2}$; it results from the action of an actuator disk which raises the head of entrained fluid from H_o to $H_o + \Delta H$.

Efforts have been directed toward the solution of the flow field generated by a heavily loaded actuator disk at zero angle of attack and to include the effects of non-uniform loading (Ref. 3), and at a finite angle of attack (Ref. 12). More directly relevant to our problem, Chaplin (Ref. 2) has investigated the performance of shrouded propellers at zero angle of attack and no forward speed. His treatment of the wake is quite similar to the one of the present work, described in Section II. A review of shrouded propeller work can be found in Weissinger and Maas' article (Ref. 9). The emphasis of this work being toward propellers, the configurations investigated are always two-dimensional axisymmetric, making the results of

use for our particular configuration as general reference only.

The potential flow model proposed in Section II is an extension of C. A. Shollenberger's analysis of the two-dimensional propulsive wing with rectilinear lifting surfaces. It accounts for camber, and in particular for flap deflection. This will be described in the next section.

II. POTENTIAL FLOW PROBLEM

1. Formulation of the Problem

This section provides the theoretical background for a numerical calculation of the potential flow around the lifting section represented in Fig. 2. It was found that the singularity system proposed in Ref. 8 for rectilinear chordlines can be extended to this more general geometry.

(a) Field Equation and Elementary Solutions

In this section, we will formulate the problem of the incompressible, inviscid homogeneous and irrotational flow about a system of lifting surfaces of specified shape in which the amount of energy addition is specified through the head change ΔH.

The lifting surfaces will be represented by cambered thin lines, in the usual thin airfoil theory formalism.

We will assume that the powered wake fluid does not substantially mix with the surrounding fluid, so that it can be assumed to be bounded by two infinitely thin vortex sheets. This assumption will model the jump in velocity between inside and outside of the wake.

In the conditions stated above, the stream function ψ of the system, and its derivatives, the velocity components u_x and u_y, satisfy the Laplace equation throughout the field (including the wake) except on the boundaries where a jump in tangential velocity occurs.

$$\nabla^2 \psi = 0$$

$$\nabla^2 u_x = \nabla^2 u_y = 0$$

We will work with the velocity components u_x and u_y because the boundary conditions are more readily expressed in terms of u_x and u_y rather than ψ.

Using the jump condition across the vortex sheet, we may decompose the tangential velocity field into a regular part, $u_{other}(x)$, due to all the other singularities in the field, and a single-valued part, representing the self-induced velocity field due to the local vorticity:

$$\lim_{y \to \pm 0} u(x, y) = u_{other} \pm u_{s \cdot i} \tag{1}$$

where $u_{si} = \frac{1}{2}\gamma(x)$ for two-dimensional vortex sheets.

Let $\vec{s} = \vec{s}(\sigma)$ specify the position of a vortex sheet (Fig. 3) of intensity $|\vec{\gamma}(\sigma)|$. Then the velocity field $\Delta\vec{u}(\vec{r})$ due to the vortex elements between σ_1 and σ_2 at any point away from the discontinuity is given by:

$$\Delta\vec{u}(\vec{r}) = \frac{1}{2\pi} \int_{\sigma_1}^{\sigma_2} \frac{\vec{\gamma}(\sigma) d\sigma \times (\vec{r} - \vec{s})}{|\vec{r} - \vec{s}|^2} \tag{2}$$

The total velocity field at that point, $\vec{u}(\vec{r})$, is found by superposing the contribution from all the vortex elements in the field. The choice of specific vortex elements is dictated by the particular problem treated. Each is referred to as an "elementary vortex" and, within this context, (2) is an elementary solution to the field equation (Poisson solution to the Laplace equation).

We have found a general expression for the solution to the field equation, expressed in terms of the singularities in that field. The next step is to find a suitable set of singularities. These are imposed by the boundary conditions.

(b) Boundary Conditions

The boundary conditions are imposed both by the airfoil surfaces and the powered wake. These can be separated into two distinct classes: those that are linear in the velocity field and those that are not.

(i) The Kinematic or Streamline Condition: Let α be the local slope of the streamline, referred to the freestream direction (local angle of attack). Then we must have the following relationship between the velocity components:

$$\frac{v_y}{U_\infty + u_x} = \tan\alpha \qquad (3)$$

Since there is no flow through the surfaces representing the airfoils, this relates the geometry of the system to the velocity field, the standard problem of thin airfoil theory.

In addition, the relation must be true in particular at the vortex sheets bounding the wake from the outside fluid. However, in this case, both α and the velocity components are a priori unknown.

Also, the presence of the powered wake imposes finite velocity perturbations at downstream infinity. We will show how this boundary condition is satisfied by the wake model we will choose.

(ii) The Pressure or Dynamic Boundary Condition in the Wake: The mixing process occurring in the ejector raises the total pressure of the entrained fluid from atmospheric head H_o to $H_o + \Delta H$. Applying the Bernoulli equation on the upper and lower side of the wake vortex sheets (Fig. 2), we get

$$H_o = p_o + \tfrac{1}{2}\rho u_o^2 \qquad \text{outside wake}$$

$$H_o + \Delta H = p_1 + \tfrac{1}{2}\rho u_1^2 \qquad \text{inside wake}$$

Continuity of static pressure across the vortex sheet requires $p_o = p_1$

$$\Delta H = \tfrac{1}{2}\rho(u_1 + u_o)(u_1 - u_o) \tag{4}$$

where ΔH is specified for this problem. Using (1), we can directly translate this into a condition for the vorticity:

$$\rho\, u_{other} \cdot \gamma(x) = \Delta H \tag{5}$$

The difficulty of satisfying this boundary condition is two-fold--it is non-linear in the velocity field, and the location at which it should be applied is a priori unknown.

The solution to the problem is completely determined, in principle, given the representation (2) of the velocity field and the set of boundary conditions (3) and (5). We must now find suitable elementary solutions and a practical scheme to actually solve the problem.

2. Vortex Distributions to Represent the Airfoil System

The chordwise distribution of vorticity in the presence of discontinuities in the shape of the boundary has been discussed extensively in Refs. 5, 6 and 16. These discontinuities occur at the leading edge, at the sharp corner representing the deflection of a flap, and possibly at the trailing edge. A singularity in the vorticity distribution at the trailing edge means flow around the trailing

edge due to jet discharge angle. This is known as "singular blowing" (Ref. 30). In our problem, the jet discharges parallel to the flap line, thus removing this condition ("regular blowing").

In the final analysis, these singularities are of two types: square root at the leading edge and logarithmic for the other two. The different nature of these singularities shows in the integrated effect: the square root singularity produces a net thrust in addition to the normal force, while the logarithmic singularity is too "weak" to produce a thrust term. It is these criteria that dictate the choice of a particular type of vortex distribution.

(a) The Leading Edge Singularity

A well-known result of thin airfoil theory is the square-root leading edge singularity of the vorticity distribution of a flat plate airfoil at an angle of attack:

$$\gamma_f(x) \sim \frac{\Gamma_f}{\sqrt{x}} \quad \text{as } x \to 0 \tag{6}$$

The flow around the leading edge of the thin section is interpreted as the limit of the flow about the round nose section of finite thickness. In both cases, this singularity produces a finite suction force $S = 2\pi\Gamma_f^2$, directed along the slope of the camberline at the leading edge.

The Kutta-Joukowsky flow about a lifting flat plate has the required behavior at the leading edge. It is described by the following analytic function:

$$w(z) = u - iv$$

$$= i\Gamma_f \left[1 - \sqrt{\frac{z-1}{z}}\right] \tag{7}$$

In particular, it gives a constant downwash $v = \Gamma_f$ on the chordline.

Further properties of this flow are listed in Appendix 1.

The chordwise distribution of vorticity for a flat plate due to the nose singularity becomes:

$$\gamma_f(x) = \Gamma_f \sqrt{\frac{1-x}{x}} \tag{8}$$

where $\tilde{\Gamma}_f = \sin\alpha$ for an isolated flat plate and is otherwise unknown for an arbitrary system (see Appendix B, page 38).

(b) The Trapezoidal Distribution of Vorticity

The logarithmic singularity occurring at flap deflection can also be handled in a similar fashion by finding the flow function due to a sharp break in the airfoil chordline. Ref. 17 has taken advantage of this approach.

In the present investigation, we found that the singularity could be adequately handled by assuming a trapezoidal distribution of vorticity between neighboring points:

$$\gamma(x) = \Gamma_i + (\Gamma_{i+1} - \Gamma_i) \cdot \frac{x}{\sigma_i} \tag{9}$$

Provided the step size σ_i is chosen small enough, the agreement in overall lift with thin airfoil theory has been found to be excellent. The pressure distribution is of course quite different in the neighborhood of the flap hinge, but then the sharp break in

camberline is not a realistic representation of the flap deflection anyway.

The field due to (9) can be calculated at any point using (2). The details of the calculation and properties of the field are listed in Appendix 1.

(c) Total Chordwise Distribution of Vorticity and Downwash

We may now superpose the contributions (8) and (9) to the vortex distribution which becomes:

$$\gamma(x_i \leq x \leq (x_i+\sigma_i)) = 2\Gamma_f \sqrt{\frac{1-x}{x}} + \Gamma_i + (\Gamma_{i+1}-\Gamma_i)\frac{x}{\sigma_i} \qquad (10)$$

where x is referred to the mean chordline of each airfoil. The resulting downwash distribution on the camberline is

$$v(x_i \leq x \leq (x_i+\sigma_i)) = \Gamma_f + \frac{1}{2\pi}\left[\Gamma_i \text{ Log } \left|\frac{x}{\sigma_i - x}\right| + (\Gamma_{i+1}-\Gamma_i)\left(-1 + \frac{x}{\sigma_i}\cdot \text{Log } \left|\frac{x}{\sigma_i - x}\right|\right)\right] + v_{other} \qquad (11)$$

The Γ_f and [ ] terms represent the downwash induced by the ith element on itself, while v_{other} represents the field generated by all the other vortex elements in the lifting system (including those on its own airfoil).

The constant term Γ_f in the downwash corresponds to a thin airfoil approximation, but it should be emphasized that the downwash component is computed at the actual location of the boundary condition on the camberline, and in the local coordinate system defined by the slope of the element at that point. In contrast, thin airfoil theories handling the downwash distribution in terms of integrals

of the vortex distribution are of necessity limited to computing the downwash as if the boundary condition were imposed at the mean-chord. Regardless of whether the approximation is justified or not, the present numerical scheme obviates the need for making it in the first place.

Having the expression of the downwash as a function of the unknown vortex distributions, we may use boundary condition (3) and solve for the distributions. This is the subject of the next section.

(d) Endpoints and Control Points on the Airfoil System

Let n be the number of segments chosen to represent the camberline for the lower airfoil, and m for the upper one.

The set of unknowns representing the vorticity of the airfoil system is:

$$\vec{G} = [\Gamma_{fl}, \Gamma_2, \ldots, \Gamma_n, \Gamma_{fu}, \ldots, \Gamma_{n+m+1}] \tag{12}$$

It contains the two leading edge singularity terms, Γ_{fl} and Γ_{fu}, and the trapezoidal terms.

We have omitted the trapezoidal terms at the leading edge of each airfoil. They may as well be taken to be zero, because the square root singularity dominates anyway. At the trailing edge, the vorticity is specified by the Kutta condition, so that $\Gamma_{n+1} = \Gamma_{n+m+2} = 0$, of course, in the unpowered case. In the powered case, the vorticity is specified otherwise; we will return to this point later.

Thus, the total number of unknown vortex intensities is the same as the total number of segments representing the system. We may select in particular the midpoints of these segments to compute the downwash, whence it takes the particularly simple form

$$v(x = \frac{\sigma}{2}) = \Gamma_f + \frac{\Gamma_i - \Gamma_{i+1}}{2\pi} + v_{other} \qquad (13)$$

We call these midpoints "control points".

We may now solve for the vortex distribution as a function of the slope of the camberline. Boundary condition (3) involves velocity components parallel and perpendicular to free-stream. Writing (13) for all (n+m) control points, and rotating to the proper coordinate system, we can write symbolically

$$u_x = U_{11}\Gamma_{f\ell} + U_{12}\Gamma_2 + \ldots + U_{1n}\Gamma_n + U_{1n+1}\Gamma_{fu} +$$

$$\ldots\ldots + U_{1n+m+1}\Gamma_{n+m+1} \equiv \underline{\underline{U}} \cdot \underline{G} \text{ for control point \#1,}$$

and similarly $u_y = \underline{\underline{V}} \cdot \underline{G}$ for all control points (14)

$\underline{\underline{U}}$ and $\underline{\underline{V}}$ are the induction functions by which given a vorticity distribution $\underline{G}$ the velocity can be calculated at any point. Conversely, given boundary condition (3) the vorticity distribution may be computed as follows:

Define $\underline{\underline{H}} = \underline{\underline{V}} - \underline{\underline{U}} \tan\alpha$

Then (3) must hold on all control points so that $\underline{\underline{H}} \cdot \underline{G} = [U_\infty \tan\alpha]$ which can be solved for $\underline{G}$:

$$\underline{G} = \underline{\underline{H}}^{-1} [U_\infty \tan\alpha] \qquad \text{Solution to the unpowered problem} \qquad (15)$$

The matrix $\underline{\underline{H}}^{-1}$ is referred to as the matrix of influence coefficients and plays an essential role in the following parts.

3. Vortex Model of the Wake

(a) General

We have seen that the difficulty of the problem arises not only from the nonlinearity of boundary condition (5), but also in the fact that the location of that boundary condition is unknown.

To obviate this difficulty, a number of investigators (Refs. 8, 2) have successfully used an iteration technique yielding a progressively better satisfaction of boundary conditions (3) and (5).

The wake is modelled by trapezoidal segments, (similar to the previous section), the position of which varies during the iteration. It must, however, be truncated after a certain downstream position. This truncation must be compatible with the boundary condition at downstream infinity mentioned previously.

(b) Representation of the Flow Field at Downstream Infinity:

The numerical scheme we are proposing involves the calculation of the downwash at arbitrary points in the field. Thus, it is a matter of practical need that we choose a representation of the flow field at downstream infinity so as to get a smooth distribution of downwash even in the last wake endpoints.

We do know that the far wake must consist of two parallel vortex sheets of vorticity $\pm\gamma_\infty = 1 - \sqrt{1+C_H}$, which is found by

applying the jump condition at $p = p_\infty$, i.e., where $u_j = U_\infty + \frac{1}{2}\gamma_\infty$. The separation of these sheets is a priori unknown otherwise. The direction is known: the far wake vortex sheets must lie along the freestream direction.

The velocity field induced by two line vortices, starting at a downstream distance x_o and separated by a distance h_∞ can then be directly computed using (2).

$$2\pi u_x = \gamma_\infty \left[\mathrm{Tan}^{-1} \left(\frac{x_o - x}{y - h_\infty} \right) - \mathrm{Tan}^{-1} \left(\frac{x_o - x}{y + h_\infty} \right) \right] \tag{16}$$

$$2\pi v_y = \gamma_\infty \, \mathrm{Log} \left[\frac{(x_o - x)^2 + (y - h_\infty)^2}{(x_o - x)^2 - (y - h_\infty)^2} \right]^{\frac{1}{2}} \tag{17}$$

where h_∞ varies during the iteration. This far wake model was also used by Shollenberger.

4. Description of the Iteration Procedure:

(a) Updating the Airfoil Vorticity:

We can conveniently separate the field components due to the wake and due to the airfoil:

$$\begin{aligned} v_y &= v_y^{(a)} + v_y^{(w)} \\ u_x &= u_x^{(a)} + u_x^{(w)} \end{aligned} \tag{18}$$

then, we may rewrite boundary condition (3) as

$$v_y^{(a)} - u_x^{(a)} \tan\alpha(x) = U_\infty \tan\alpha(x) + u_x^{(w)} \tan\alpha(x) - v_y^{(w)} \tag{19}$$

The field at the control points is expressed as: $\underline{\underline{H}} \cdot \underline{G}$, where $\underline{G}$ is to be determined. Then, the amount of vorticity imbedded in the

airfoil required to satisfy the boundary condition in the presence of the wake-induced velocity components will be

$$\underline{G} = \underline{\underline{H}}^{-1} \cdot [U_\infty \tan\alpha + u_x^{(w)} \tan\alpha - v_y^{(w)}] \tag{20}$$

$\underline{\underline{H}}^{-1}$ is independent of the iteration and is calculated once and for all for $C_H = 0$.

(b) Updating the Wake

(i) Updating the Position. To find the slope of the vortex sheet at the control point, we observe that if indeed this slope were actually known, then it would be continuous across the vortex sheet, i.e.:

$$\frac{u_{x1}}{v_{y1}} = \frac{u_{xo}}{v_{yo}} = \tan\alpha(x) \tag{21}$$

(1 and 0 referring to the velocities inside and outside the wake).

So that since $1 + \dfrac{u_{x1}}{v_{y1}} = 1 + \dfrac{u_{xo}}{v_{yo}}$

and $$\tan\alpha(x) = \frac{u_{xo}+u_{x1}}{v_{yo}+v_{y1}} = \frac{u_{xo}}{v_{yo}} \tag{22}$$

Now, we want to use the jump condition across the vortex so we must transform to a system parallel to the vortex.

$$u_x = u \cos\alpha(x) - v \sin\alpha(x)$$

$$v_y = u \sin\alpha(x) + v \cos\alpha(x)$$

for u_o and u_1

where

$$u_o = u_{other} - \tfrac{1}{2}\gamma(x)$$

$$u_1 = u_{other} + \tfrac{1}{2}\gamma(x)$$

so that

$$u_o + u_1 = 2\,u_{other}$$

$$v = v_{other} + v_{s.i.}$$

$$\tan\alpha(x) = \frac{2\,u_{other}\sin\alpha + (v_{other}+v_{si})\cos\alpha}{2\,u_{other}\cos\alpha - (v_{other}+v_{si})\sin\alpha} \tag{23}$$

If the boundary condition is exactly satisfied, then $v_N = v_{other} + v_{si}$, which represents the total velocity normal to the vortex sheet, will be zero, so that (23) is satisfied identically.

If the boundary condition is not exactly satisfied, then $v_N \neq 0$ and a better estimate of the slope can be found by using (23) as:

$$\tan\alpha^{(new)} = \frac{2u_{other}^{(new)} \cdot \sin\alpha^{(old)} + (v_{other}^{(new)} + v_{si}^{(new)}) \cdot \cos\alpha^{(old)}}{2u_{other}^{(new)} \cos\alpha^{(old)} - (v_{other}^{(new)} + v_{si}^{(new)}) \cdot \sin\alpha^{(old)}} \tag{24}$$

Having executed that for all the control points in the wake, we can find the new wake position by direct integration:

$$y_w(x) = y_{TE} + \int_{x_{TE}}^{x} \tan\alpha(x')dx' \tag{25}$$

(ii) Updating the Vorticity: The updating of the vorticity at the control points is readily obtained by using boundary condition (5). The vorticity at the endpoints is then obtained by averaging the vorticity between neighboring endpoints. The exceptions to this rule

are:

(1) at the trailing edge of the airfoil, the vorticity is linearly extrapolated from the first wake control point. The continuity of vorticity at this point complies with the Kutta condition for regular blowing.

(2) the vorticity of the two last wake endpoints is set to $\pm\gamma_\infty$.

5. Computation of the Aerodynamic Coefficients

(a) Forces

Definitions:

We will call "lift" any force component perpendicular to the freestream direction, and "thrust" any component parallel but opposite to the freestream direction (i.e., thrust is measured by negative numbers and drag by positive numbers).

(i) The leading edge suction term can be found explicitly by integrating the flat plate vorticity term around a lip of finite radius and then letting the radius go to zero. The leading edge suction is then

$$C_s = -2\pi \tilde{\Gamma}_f^2 \qquad \text{for each airfoil} \tag{26}$$

and acts tangentially to the leading edge element.

This thrust, of course, does not produce any moment about the leading edge.

(ii) The Pressure Integral Across the Camberline. This is the only place where the actual location of the actuator disk enters, since the Bernoulli equation involves explicitly the head of the flow.

For convenience, we assume that the actuator disk is located at the trailing edge of the system, so that the fluid is assumed to be at atmospheric head H_o up to that point. This certainly does not affect the value of the total lift on the system, since it depends only on the total amount of vorticity shed by the actuator disk, but will affect the distribution of lift between the two airfoils and the load. However, to represent these realistically would require detailed knowledge of the mixing zone, unavailable at the present time. To find the pressure difference acting between x_i and x_{i+1} on the element of the camberline, we apply the Bernoulli equation on its upper and lower side.

$$p_L - p_\infty = \tfrac{1}{2}\rho U_\infty^2 - \tfrac{1}{2}\rho[\,u_{other}(x) - u'\,]^2$$

$$p_u - p_\infty = \tfrac{1}{2}\rho U_\infty^2 - \tfrac{1}{2}\rho\,[\,u_{other}(x) + u'\,]^2 \qquad (27)$$

where $u' = -\tfrac{1}{2}\gamma(x)$; thus the load is $\Delta p = \tfrac{1}{2}\rho(4\, u_{other} u')$. (28)

The elementary normal force acting on the element is:

$$N_{ti} = \int_{x_i}^{x_{i+1}} \Delta p \, dx$$

$$= +\rho \int_{x_i}^{x_{i+1}} u_{other}(x)\gamma(x)dx$$

$u_{other}(x)$ is the contribution of all the other vortices in the field, and does not vary much over segment i. It is most convenient to compute the velocity at the control point between x_i and x_{i+1}. Thus, normalizing as usual:

$$\tilde{N}_{ti} = + 2\tilde{U}\,(x_i + \frac{\sigma_i}{2}) \cdot \int_{x_i}^{x_{i+1}} \tilde{\gamma}(x)\,dx$$

This component contributes both to the overall thrust and lift of the system. It is more convenient to refer this component to the mean chord coordinates. Let ε_i = slope of the camberline in these coordinates. Then:

$$\tilde{N}_i = \cos \varepsilon_i \, \tilde{N}_{ti}$$

$$\tilde{T}_i = - \sin \varepsilon_i \, \tilde{N}_{ti} \qquad (29)$$

Using the representation of the vorticity (10), we can integrate the vorticity term

$$\int_{x_i}^{x_{i+1}} \tilde{\gamma}(x)dx = \tilde{\Gamma}_f [(\theta_{i+1} - \theta_i) + (\sin\theta_{i+1} - \sin\theta_i)]$$

$$+ \tfrac{1}{2}[\tilde{\Gamma}_{i+1} + \tilde{\Gamma}_i] \cdot \Delta x_i \qquad (30)$$

where $\theta = \text{Arc}\cos(\frac{2x}{c} - 1)$.

Including the leading edge suction term, (26), the total normal and tangential referred to the airfoil mean line become:

$$\tilde{N} = -2\pi \tilde{\Gamma}_f^2 \sin\beta + \sum_{i=1}^{n} \tilde{N}_i$$

$$\tilde{T} = -2\pi \tilde{\Gamma}_f^2 \cos\beta + \sum_{i=1}^{n} \tilde{T}_i \qquad (31)$$

(β is the slope of the camberline at the leading edge $\beta = \varepsilon_1$.)

To obtain the lift and thrust coefficients we rotate to the freestream coordinates:

$$C_L = \tilde{N} \cdot \cos(\alpha+\beta) - \tilde{T} \sin(\alpha+\beta)$$

$$C_T = \tilde{N} \cdot \sin(\alpha+\beta) + \tilde{T} \cos(\alpha+\beta) \qquad (32)$$

(iii) The Pressure Integral on the Actuator Disk. The forces due to the actuator disk (for the case of uniform loading) (referring to Fig. 8) are simply its normal thrust referred to the thrust and lift directions defined previously:

$$C_{L_A} = C_H \cdot h \cdot \sin(\alpha+\delta)$$

$$C_{T_A} = -C_H \cdot h \cdot \cos(\alpha+\delta) \qquad (33)$$

So that finally we obtain the total lift and thrust coefficient acting on the system:

$$C_{L_{tot}} = C_{L_1} + C_{L_2} + C_{L_A}$$

$$C_{T_{tot}} = C_{T_1} + C_{T_2} + C_{T_A} \qquad (34)$$

It is these coefficients characteristic of the total vorticity in the field (airfoil + wake) that are significant in the comparison with jet-flap theory.

(b) Moments

We refer all our moments to the leading edge of the main airfoil. In this definition the nose thrust of the main airfoil does not contribute to the moment of the system, but the nose thrust of the shroud does.

(i) Main Airfoil. Referring to Fig. 8, the contribution of the ith element to the moment about the nose is

$$\tilde{M}_i = \int_{x_i}^{x_{i+1}} x d\tilde{N}_i - \int_{y_i}^{y_{i+1}} y d\tilde{T}_i \tag{35}$$

where

$$d\tilde{N}_i = \cos\varepsilon_i \cdot d\tilde{N}_{ti}$$

$$d\tilde{T}_i = -\sin\varepsilon_i \, d\tilde{N}_{ti} \tag{36}$$

and y is related to x by the local slope of the camberline: $y(x) = x\tan\varepsilon_i + y_i - x_i \tan\varepsilon_i$. Making the same approximation as in (a) concerning the velocity, we get, after some manipulation:

$$\tilde{M}^{(i)} = +2\tilde{U}(x_i + \tfrac{i}{2}) \cdot [\cos\varepsilon_i + \sin\varepsilon_i \tan\varepsilon_i] \cdot \int_{x_i}^{x_{i+1}} x\tilde{\gamma}(x)dx$$

$$- (y_i - x_i \tan\varepsilon_i)\,\tilde{T}^{(i)} \tag{37}$$

Writing the vorticity integral explicitly:

$$\int_{x_i}^{x_{i+1}} x\tilde{\gamma}(x)dx = \tfrac{1}{4}\tilde{\Gamma}_f[\theta_{i+1} - \theta_i - \tfrac{1}{2}(\sin 2\theta_{i+1} - \sin 2\theta_i)] +$$

$$+ \tfrac{1}{2}\tilde{\Gamma}_i (x_{i+1}^2 - x_i^2) + \frac{\tilde{\Gamma}_{i+1} - \tilde{\Gamma}_i}{x_{i+1} - x_i}\left[\tfrac{1}{3}x_{i+1}^3 + \tfrac{1}{6}x_i^3 - \tfrac{1}{2}x_i x_{i+1}\right] \tag{38}$$

The total moment acting about the nose due to the lower airfoil becomes:

$$C_{M_l} = \sum_{i=1}^{n} \tilde{M}^{(i)} \tag{39}$$

(ii) Moment Due to the Shroud

Moment due to the normal force on the shroud. We assume that the maximum camber of the shroud airfoil is small enough so that we may neglect the local slope in computing the moment about the leading edge of the shroud, i.e. (referring to Fig. 8)

$$M_1 = \int_{x_1}^{x_2} x' \cdot \left(\frac{dN}{dx'}\right) dx' \tag{40}$$

and then the moment transferred to the leading edge of the main airfoil becomes:

$$M_o = \int_{x_1}^{x_2} x dF_y - \int_{y_1}^{y_2} y dF_x \tag{41}$$

using

$$\tan\varepsilon_M = \frac{y_2 - y_1}{x_2 - x} \tag{42}$$

$$\begin{aligned} dF_y &= dN \cos\varepsilon_M \\ dF_x &= -dN \sin\varepsilon_M \end{aligned} \tag{43}$$

we finally get:

$$C_{M_2} = M_o(N) = M_1(N) + [x_1 \cdot \cos\varepsilon_M + y_1 \cdot \sin\varepsilon_M] \cdot |\tilde{N}| \tag{44}$$

where (x_1, y_1) is the position of the nose of the shroud in the main airfoil coordinates.

We must add to this the moment due to the leading edge suction, which is readily found to be

$$M_o(s_{LE}) = 2\pi\tilde{\Gamma}_f^2 \left[y_1 \cos\varepsilon_M - x_1 \sin\varepsilon_M\right] \tag{45}$$

(iii) Moment Due to Actuator. Referring to Fig. 8, the contribution to the moment due to the actuator is found to be independent of the position of the actuator and

$$C_{M_{act}} = C_H \, h.d \tag{46}$$

where d is the lever arm of the actuator. The total moment can be found by simply adding the various contributions:

$$C_{M_{tot}} = C_{M_1} + C_{M_2} + M_o(S_{le}) + C_{M_{act}} \tag{47}$$

6. Performance of Numerical Scheme

The numerical calculations were performed on the IBM/System 370 available at the CIT Computing Center.

45 segments were chosen to represent the camberline of the test configuration. The total computing time for the unpowered configuration, including the inversion of the influence coefficients matrix, was about 20 seconds.

The step size of the segments selected to represent the wake must be smaller than or equal to the exit height of the ejector, $\frac{h}{c}$. For a fixed downstream wake cutoff distance, low $\frac{h}{c}$ ratios translate into a larger number of segments to insure convergence, resulting in an increase of the required computing time. Thus, for a $\frac{h}{c} = 15\%$ and wake cutoff at 5 chords downstream, 50 segments were used.

The number of iterations required for a given accuracy in the aerodynamic coefficients appear to be directly proportional to C_H, and sensitive to a lesser degree to an increase in the angle of

attack and/or flap deflection.

For the case of high C_H and low $\frac{h}{c}$, the total amount of computing time for a complete set of iterations is about 2 minutes.

III. COMPARISON WITH JET-FLAP THEORY

In a well-known paper (Ref. 6), Spence developed a linearized theory for the two-dimensional potential flow about a single element jet-flap airfoil and computed the lift increment due to blowing in the form of lift derivatives tabulated versus the jet momentum coefficient of the primary C_μ. In the previous section, we proposed a numerical scheme to compute the lift coefficient on a multi-element airfoil, given the head change C_H. The purpose of this section is to establish a technique for the comparison between the lift increments obtained by the two different methods.

1. General Characteristics of the Computed Lift Curves

For a constant flap deflection, the functional dependence of the lift coefficient can be written as:

$$C_L = C_L(\alpha, C_H) \tag{48}$$

so that

$$C_L = C_L(\alpha = 0°, C_H=0) + \frac{\partial C_L}{\partial \alpha}\Big|_{C_H} \cdot \alpha + \frac{\partial C_L}{\partial C_H}\Big|_{\alpha} \cdot C_H \tag{49}$$

(neglecting cross-terms)

We may regroup

$$C_L(\alpha = 0°, C_H) = C_L(\alpha = 0°, C_H = 0) + \frac{\partial C_L}{\partial C_H} \cdot C_H \tag{50}$$

so that the lift increment due to angle of attack only becomes

$$\Delta C_L = \frac{\partial C_L}{\partial \alpha}\Big|_{C_H} \alpha$$

$$= C_L - C_L(\alpha = 0°, C_H) \tag{51}$$

The presence of a finite lift at zero angle of attack in the powered case results from the asymmetry in the lifting surfaces. In the early part of the work, some difficulty was encountered in the interpretation of the lift curves, because a finite lift at $\alpha = 0°$ results in lift derivatives (as computed directly from (48)) becoming infinite at that angle, thus precluding any meaningful comparison with Spence's theory.

Dr. H. J. Stewart recognized the similarity of this behavior with that of a wing equipped with suction-type boundary-layer control, of which he previously made the theory for a single element airfoil (Ref. 18). This theory will be repeated below, and affords a direct interpretation of the lift curves at $\alpha = 0°$.

Having established that, it will then be shown that the lift increment due to angle of attack only can be directly related to Spence's increment, having suitably related the head change C_H to the total momentum flowing in the wake.

2. Effect of a Sink on a Single-element Airfoil

The suction effect of a boundary layer control device can be represented by a sink on the upper side of the airfoil. (Fig. 10) The analysis of this effect was done in Ref. 18 and is repeated here, as it provides the theoretical background necessary to interpret the presence in our configuration of finite lift at $\alpha = 0°$. In the transformed plane, the combination of sources and sinks necessary to maintain the circle a streamline is also shown in Fig. 10. Let θ be the angle between the direction of the sinks and the rear stagnation point. Let the distance between the sinks go to zero. Then, the

horizontal velocity component generated by the sink of strength -2Q is cancelled by the velocity due to the source +Q at the origin. The net vertical velocity component is given by:

$$v_y = \frac{2Q}{2\pi(2R \sin\frac{\theta}{2})} \cos(\frac{\theta}{2}) \tag{52}$$

$$= \frac{Q}{2\pi R} \cot(\frac{\theta}{2}) \tag{53}$$

Thus, to maintain the stagnation point at the trailing edge, an extra amount $\Delta\Gamma_{ind}$ of vorticity at the center of the circle is necessary, directed counter-clockwise so that its induced velocity component exactly cancels (53):

$$\frac{\Delta\Gamma_{ind}}{2\pi R} = \frac{Q}{2\pi R} \cdot \cot(\frac{\theta}{2}) \Rightarrow \Delta\Gamma_{ind} = Q \cot(\frac{\theta}{2}) \tag{54}$$

The resulting lift increment is $\rho U_\infty \Delta\Gamma_{ind}$. The total lift becomes:

$$L = \pi\rho U_\infty^2 c\sin\alpha + \rho U_\infty \cdot Q \cot(\frac{\theta}{2}) \tag{55}$$

and in particular is nonzero as $\alpha = 0^\circ$.

3. Comparison with the Computed Lift Curves at $\alpha = 0^\circ$: the Actuator as a Sink

To relate this to our configuration, we must first estimate Q as a function of C_H. The strength of the sink is the difference in mass flux between the power-on and power-off configuration, which can be estimated as:

$$-Q = hU_\infty - hu_j$$

$$= hU_\infty \left[1 - (1 + C_H)^{\frac{1}{2}}\right] \tag{56}$$

Also, we recognize that the $\cot(\frac{\theta}{2})$ factor is valid only for a single element airfoil. For a multiple element airfoil, we expect that the factor should be somewhat different. In particular, if the two chords are equal, then the symmetry of the problem dictates that there can be no lift at $\alpha = 0^\circ$. Thus, the estimate of the lift increment becomes:

$$\Delta C_{L_{ind}} = 2k(\frac{c_u}{c}, \frac{h}{c}) \left[(1 + C_H)^{\frac{1}{2}} - 1\right] \tag{57}$$

where the factor $k(\frac{c_u}{c}, \frac{h}{c})$ must be determined for the particular geometry considered.

The lift slope computed numerically in Fig. 11 corresponds to a system having a chord ratio $\frac{c_u}{c} = 40\%$ and an ejector height $\frac{h}{c} = 15\%$. The numerical value of coefficient k was determined by a best fit of the curves $C_L(\alpha = 0^\circ, C_H)$ and $\Delta C_{L_{ind}}$, which was obtained for $k = .1625$. The agreement between the two curves validates the interpretation proposed for the mechanism of generation of lift at $\alpha = 0^\circ$.

4. Comparison of the Lift Increments Due to Angle of Attack with Spence's Theory

The lift increment due to angle of attack computed numerically by Spence in Ref. 6 can be approximated by

$$\Delta C_{L_{JF}} = 2\pi \left[1 + .151\ C_J^{\frac{1}{2}} + .219\ C_J\right] \alpha \qquad (58)$$

(no lift at $\alpha = 0°$)

where C_J is the momentum flowing in the powered wake. For a jet flap, this is just equal to the momentum of the primary $C_J = C_\mu$, as this model neglects any entrainment in that region. To relate $\Delta C_{L_{JF}}$ to the lift increments computed in our configuration, we must relate C_J to C_H.

a. Relation Between Head Change and Momentum Coefficient

Referring to Fig. 2, the total momentum flow in the far wake is:

$$M = \rho\, u_j^2\, h_\infty$$

where u_j is related to the head change by

$$p_\infty + \tfrac{1}{2}\rho U_\infty^2 + \Delta H = p_\infty + \tfrac{1}{2}\rho u_j^2$$

so that

$$\rho u_j^2 = \rho U_\infty^2 + 2\Delta H$$

and

$$M = h_\infty \left[\rho U_\infty^2 + 2\Delta H\right] \qquad (59)$$

For the type of geometries representative of an ejector-powered jet-flap, the exit height to chord ratio $\frac{h_s}{c}$ will be of the order of 10%. Under these conditions, the results of the numerical

scheme proposed in Section II show no appreciable slipstream contraction, i.e., $\frac{h_s}{h_\infty} \approx 1$. This allows us to neglect the pressure integral on the wake and identify (59) with the total momentum flow at the exit of the ejector:

$$M_s = h_s \left[\rho U_\infty^2 + 2\Delta H\right]$$

so that the jet coefficient that will be used in the comparison with Spence's theory will be

$$\begin{aligned} C_J &= \frac{M_s}{\frac{1}{2}\rho U_\infty^2 c} \\ &= 2\frac{h_s}{c} + 2 \cdot \frac{\Delta H}{\frac{1}{2}\rho U_\infty^2} \frac{h_s}{c} \\ &= 2\frac{h_s}{c}\left[1+C_H\right] \end{aligned} \tag{60}$$

To relate C_J to the conventional primary jet momentum C_μ, we note that C_H is the force, i.e., change in momentum, exerted per unit height by the actuator disk on the pumped fluid, so that

$$C_\mu = \frac{h_s}{c} C_H \tag{61}$$

and

$$C_J = 2\frac{h_s}{c} + 2\, C_\mu \tag{62}$$

A further implication of this choice is clear when we consider the ejector at zero forward speed $U_\infty = 0$

so that (51) $\Rightarrow M_J = 2M_\mu$

and

$$\frac{M_J}{M_\mu} = 2$$

This ideal augmentation coefficient can be achieved only by an ideal mixing device (Ref. 21).

b. Comparison of the Lift Increments

We are now in a position to compare the lift increments due to angle of attack computed by the two methods. This has been done in Figures 11 and 12 by comparing the lift curve obtained numerically and the curve $C_L = C_L(\alpha = 0°, C_H) + \Delta C_{L_{JF}}$, where $C_L(\alpha = 0°, C_H)$ is also computed numerically, for the following configurations (the geometries are in Fig. 2-A):

Fig. 11. System of unflapped flat-plate airfoils, with height $\frac{h}{c} = 15\%$ and chord ratio $\frac{c_u}{c} = 40\%$

Fig. 12. System of flapped cambered sections corresponding to a configuration tested in the 10-foot tunnel at GALCIT and described in Ref. 34.

It is seen that for these widely different configurations the lift increments computed by both methods agree quite well. In addition, the distribution of lift between the two airfoils has been plotted in Figs. 15 and 16 for an actuator disk effectively located at the trailing edge of the system. Both lift slopes are negative, indicating the presence of the upper airfoil stagnation point on its upper surface. This again illustrates the sink effect of the actuator on the lifting surfaces.

5. Comparison of the Moment Curves

A similar comparison was made for the moment curves of the same configurations as above, the moment increment being also obtained from Ref. 6.

For the flat-plate system (Fig. 13), the curves have different slopes and cross for a value of C_H high enough.

For the cambered system (Fig. 14), the magnitude of the moment increment as well as the slopes agree with the moment increment computed from Ref. 6.

To the extent of this comparison, this indicates that the moment increment is sensitive to the particular geometry considered and cannot in general be reliably computed from the jet flap increment.

6. Conclusions

The method of superposition that has been just discussed allows a simple interpretation of the lift curves computed numerically in terms of analytical results for single-airfoil configurations. While it does not remove the need to compute numerically the lift at $\alpha = 0°$, it lends to the numerical solution a flexibility that is inherently lacking in this type of approach.

APPENDIX

A. The Trapezoidal Vorticity

1. Expression for the Flow Field

Let σ_i be the mesh size $\sigma_i = x_{i+1} - x_i$.

The trapezoidal vorticity is a linear distribution of vorticity between x_i and x_{i+1}.

$$\gamma(x) = \Gamma_i + (\Gamma_{i+1} - \Gamma_i) \cdot \frac{x}{\sigma_i} \tag{1-1}$$

We want to compute the induced velocity using the Biot Savart law:

$$dur = \frac{\gamma(x)dx}{2\pi r} \tag{1-2}$$

$$2\pi u_x = \int_o^\sigma \frac{-\gamma(x)\cdot y}{r^2}\, dx \tag{1-3}$$

$$2\pi u_y = \int_o^\sigma \frac{x'-x}{r^2}\, \gamma(x)dx \tag{1-4}$$

Carrying out the integration:

$$2\pi u_x = \Gamma_i \cdot \left[\mathrm{Tan}^{-1}\left(\frac{x-\sigma_i}{y}\right) - \mathrm{Tan}^{-1}\left(\frac{x}{y}\right)\right] +$$

$$+(\Gamma_{i+1}-\Gamma_i)\cdot\left\{\frac{y}{\sigma_i}\,\mathrm{Log}\left[\frac{x^2+y^2}{(\sigma_i-x)^2+y^2}\right]^{\frac{1}{2}} + \frac{x}{\sigma_i}\left[\mathrm{Tan}^{-1}\left(\frac{x-\sigma_i}{y}\right) - \mathrm{Tan}^{-1}\left(\frac{x}{y}\right)\right]\right. \tag{1-5}$$

$$2\pi u_y = \Gamma_i\,\mathrm{Log}\left[\frac{x^2+y^2}{(\sigma_i-x)^2+y^2}\right]^{\frac{1}{2}} +$$

$$+(\Gamma_{i+1}-\Gamma_i)\cdot\left\{-1+\frac{x}{\sigma_i}\,\mathrm{Log}\left[\frac{x^2+y^2}{(\sigma_i-x)^2+y^2}\right]^{\frac{1}{2}} - \frac{y}{\sigma_i}\left[\mathrm{Tan}^{-1}\left(\frac{x-\sigma_i}{y}\right) - \mathrm{Tan}^{-1}\left(\frac{x}{y}\right)\right]\right\} \tag{1-6}$$

2. Limit Forms of (1-5) and (1-6) as $y \to \pm 0$

(i) $x<0$ or $x>\sigma$ $\quad \mathrm{Tan}^{-1}\left(\frac{x-\sigma_i}{y}\right)-\mathrm{Tan}^{-1}\left(\frac{x}{y}\right)\to \pm\frac{\pi}{2}-\left(\pm\frac{\pi}{2}\right)=0 \qquad (1\text{-}7)$

$\therefore\ 2\pi u_x = 0$

$$2\pi u_y = \Gamma_i \mathrm{Log}\left|\frac{x}{\sigma_i - x}\right| + (\Gamma_{i+1}-\Gamma_i)\left\{-1+\frac{x}{\sigma_i}\mathrm{Log}\left|\frac{x}{\sigma_i - x}\right|\right\}$$

Same holds for $x > \sigma_i$

(ii) $0 < x < \sigma_i$

$$\mathrm{Tan}^{-1}\left(\frac{x}{y}\right) - \mathrm{Tan}^{-1}\left(\frac{x-\sigma_i}{y}\right) \to \pm\frac{\pi}{2} + \left(\pm\frac{\pi}{2}\right) = \pm\pi$$

So that $u_x(0< x < \sigma_i,\ y = \pm 0) = \pm\frac{1}{2}\gamma(x) \qquad (1\text{-}8)$

(iii) Expression for the downwash

In computing the downwash, we require $u_x = 0$ so that

$$2\pi u_y = \Gamma_i \mathrm{Log}\left|\frac{x}{\sigma_i - x}\right| + (\Gamma_{i+1}-\Gamma_i)\cdot\left[-1+\frac{x}{\sigma_i}\mathrm{Log}\left|\frac{x}{\sigma_i - x}\right|\right]$$

and in particular (1-9) evaluated at the midpoint yields:

$$u_y\left(x' = \frac{\sigma}{2},\ y' = 0\right) = -\frac{1}{2\pi}(\Gamma_{i+1}-\Gamma_i) \qquad (1\text{-}10)$$

3. Comment

It should not be concluded that the field at the end of these segments $x = \sigma$ is inherently singular, since the downwash is computed as $v = v_{si} + v_{other}$ although, should one need the downwash at that particular point to interface with a complete integral model of the turbulent flow outside the ejector additional numerical sophistication would be needed.

B. Field of the Leading Edge Singularity

The Kutta-Joukowsky flow about a lifting flat plate is represented by

$$w(z) = u - iv$$

$$= i\,\tilde{\Gamma}_f \left[1 - \sqrt{\frac{z-1}{z}}\right] \tag{1-11}$$

where $\tilde{\Gamma}_f =$ sina for an isolated flat plate.

Using the angles in Fig. 5, this can be decomposed into real and imaginary parts

$$R^2 = (1-x)^2 + y^2$$

$$r^2 = x^2 + y^2 \tag{1-12}$$

Then

$$u = \tilde{\Gamma}_f \cdot \left[\frac{R^{\frac{1}{2}}}{r^{\frac{1}{2}}} \sin\gamma\right] \tag{1-13}$$

$y \geq 0$

$$v = \tilde{\Gamma}_f \left[1 - \frac{R^{\frac{1}{2}}}{r^{\frac{1}{2}}} \cos\gamma\right] \tag{1-14}$$

where $\gamma = \dfrac{\theta_2 - \theta_1}{2}$

The downwash on the chordline $y = 0$, $0 \leq x \leq 1$, is constant : $v = \tilde{\Gamma}_f$.

Outside this interval, on the line through the two branch points, we have

$$v = \tilde{\Gamma}_f \cdot \left[1 - \sqrt{\frac{x-1}{x}}\right], \quad x < 0 \quad \text{and} \quad x \geq 1$$

In addition, the vorticity distribution can be deduced from (11) and is,

$$\gamma_f(0 \leq x \leq 1) = 2\Gamma_f \cdot \sqrt{\frac{1-x}{x}} \qquad (1\text{-}15)$$

with the square root singularity at the leading edge.

The complex function (1-11) represents the leading edge singularity for any thin airfoil as well as for a flat plate, provided the branch cut is moved to coincide with the camberline. In the particular scheme we used for the numerical solution, the branch cut was not moved, so that the contribution of the leading edge singularity to the total downwash on its own airfoil, given in equation (11), is just $\tilde{\Gamma}_f$, and the vorticity is (1-15). These two results are linearized approximations. The nonlinear results could have been incorporated at a slight increase in the complexity of the calculation. A consistency check was made by computing the velocity components directly from the computed vorticity distribution equation (15), and they satisfied the imposed boundary condition within three significant digits. Thus, in this particular example, this approximation was well justified.

REFERENCES

1. Herold, Alan C., A Two-dimensional, Iterative Solution for the Jet Flap, NASA CR-2190.
2. Chaplin, H. R., A Method for the Numerical Calculation of Slipstream Contraction of a Shrouded Impulse Disk in the Static Case, DTMB Rept. 1857, June 1964.
3. Greenberg, Michael D., Powers, Stephen R., Non-Linear Actuator Disk Theory and Flow Field Calculations, Including Non Uniform Loading, NASA CR-1672.
4. von Karman, Th., Burgers, J. M., Aerodynamic Theory, Durand, ed., Vol. II, Perfect Fluids, Section 10.
5. Spence, D. A., The Lift Coefficient of a Thin, Jet Flapped Wing, Proc. Royal Soc. A 238, 1956.
6. Spence, D. A., Some Simple Results for 2-D Jet Flap Aerofoils., Aero Quarterly, Nov. 1958.
7. Wygnanski, I., Newman, B. G., The Effect of Jet Entrainment on Lift and Moment for a Thin Airfoil with Blowing, Aero Quarterly, May 1964.
8. Shollenberger, Carl A., An Investigation of a 2-D Propulsive System, Calif. Inst. of Technology, Ph.D. Thesis, 1971.
9. Weissinger, Johannes, Maas, Dieter, Theory of the Ducted Propeller - A Review. Article in 7th Symposium on Naval Hydrodynamics, Aug. 25-30, 1968.
10. Yen, K. T., On the Thrust Hypothesis for the Jet Flap, Including Jet-Mixing Effects, Journal of the Aerospace Sciences, Aug. 1960.

REFERENCES (Cont'd)

11. Stratford, B. S., Early Thoughts on the Jet Flap, Aero Quarterly 7, 1956.

12. Levinsky, E. S., et al., Lifting Theory for V/STOL Aircraft in Transition and Cruise I., J. of Aircraft, Vol. 6, No. 6.

13. Spence, D. A., The Lift Coefficient of a Thin Jet-Flapped Wing. II. A Solution of the Integro-differential Equation for the Slope of the Jet., Proc. Roy. Soc., Series A 261.

14. Stratford, B. S., Mixing and the Jet Flap, Aero Quarterly, Vol. VII, May 1956.

15. Stratford, B. S., A Further Discussion on the Mixing and the Jet Flap,

16. Lissaman, P. B. S., A Linear Solution for the Jet Flap in Ground Effect, Ph.D. Thesis, Calif. Inst. of Technology, 1965.

17. Lopez, M. L., Shen, C. C., Recent Developments in Jet Flap Theory and Its Application to STOL Aerodynamic Analysis, AIAA Paper 71-578.

18. Stewart, H. J., Private Communication.

19. Quinn, Brian, A Wind Tunnel Investigation of the Forces Acting on an Ejector in Flight, ARL Rept. 70-0141.

20. Fancher, R. B., Why Ejectors for Aircraft Propulsion-Lift Systems and Where We Stand, ARL Rept. 71-0140.

21. von Karman, T., Theoretical Remarks on Thrust Augmentation. Reissner Anniversary Volume, J. W. Edwards, 1949.

REFERENCES (Cont'd)

22. Steady Flow Ejector Research Program. Final Report Contract Nonr-3067(00), Dec. 1960.

23. Curtet, Roger, Thèse, Faculté des Sciences de l'Université de Grenoble, Nov. 1958, Publ. Sc. and Tech au Min de l'Air, No. 106.

24. Rose, James R., Ph. D. Thesis, Calif. Inst. of Technology, An Analysis of the 2-D, Incompressible Jet Ejector, 1969.

25. Hill, P. G., Turbulent Jets in Ducted Streams, JFM 22, 1965.

26. Koenig, David G., Corsiglia, Victor R., Aerodynamic Characteristics of a Large Scale Model with an Unswept Wing and Augmented Jet Flap, NASA TN D-4610, 1968.

27. Cook, A. M., Aiken, T. N., Low Speed Aerodynamic Characteristics of a Large Scale STOL Transport Model with an Augmented Jet Flap, NASA TM X62017, 1971.

28. Flight International, Boeing's AMST Proposal, 8 Feb. 1973, p. 210.

29. Perry, D. H., A Review of Some Published Data on the External-Flow Jet-Augmented Flap, Aeronautical Research Council Current Papers, CP No. 1194, London, 1972.

30. Lachmann, G. V., ed., Boundary Layer and Flow Control, Vol. I, Pergamon Press, London, 1961.

31. McCormack, Barnes W., Jr., Aerodynamics of V/STOL Flight, Academic Press, New York, 1967.

32. Harris, G. L. and Lissaman, P. B. S., The Mechanics of Ejector Thrust Augmentation, CIT Ae TR 67-1, 1967.

REFERENCES (Cont'd)

33. Newman, B. G., The Prediction of Turbulent Jets and Wall Jets, Canadian Aeronautics and Space Journal, October 1969.

34. GALCIT Report 926 (to be published).

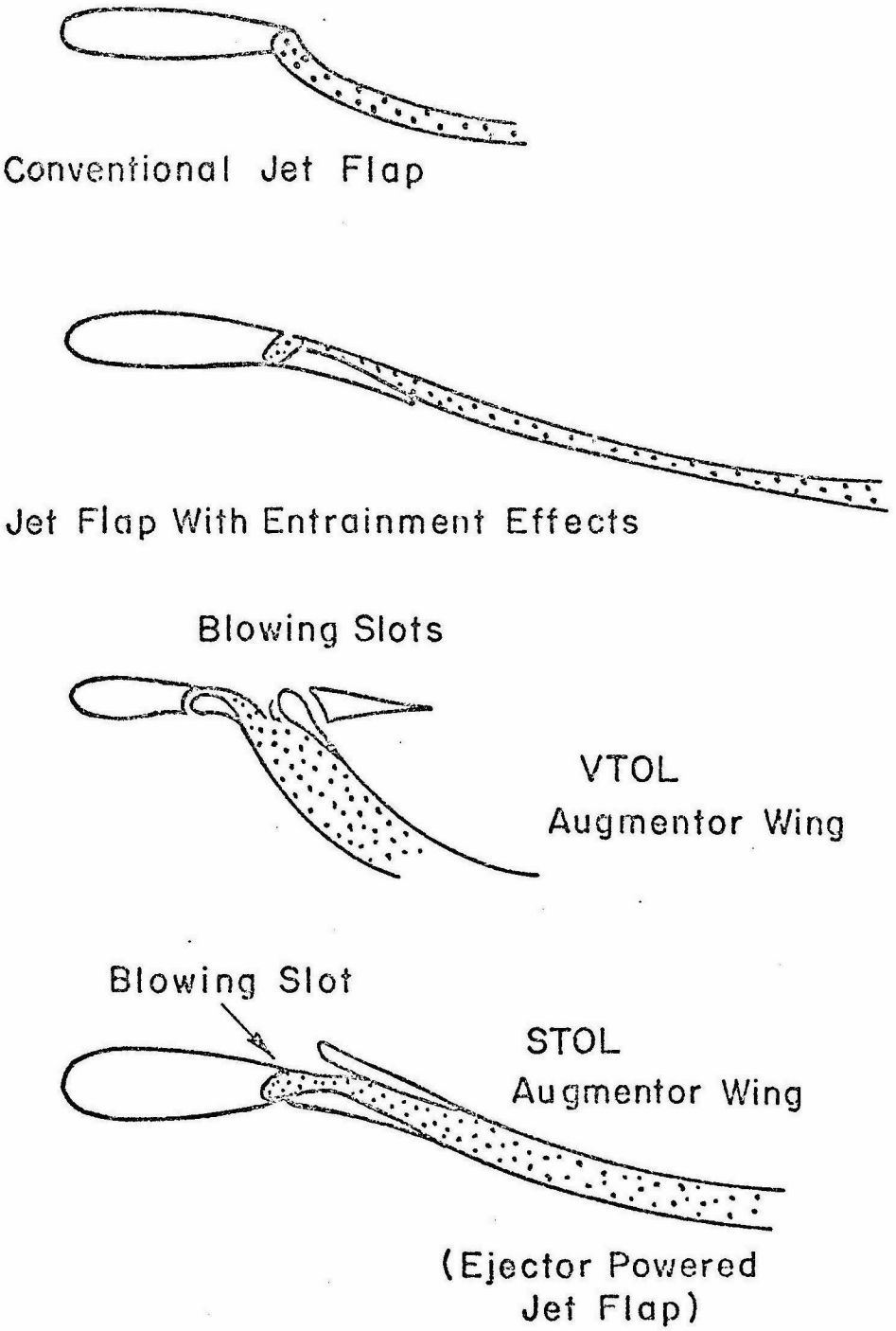

FIG. 1 POWERED LIFTING SYSTEMS

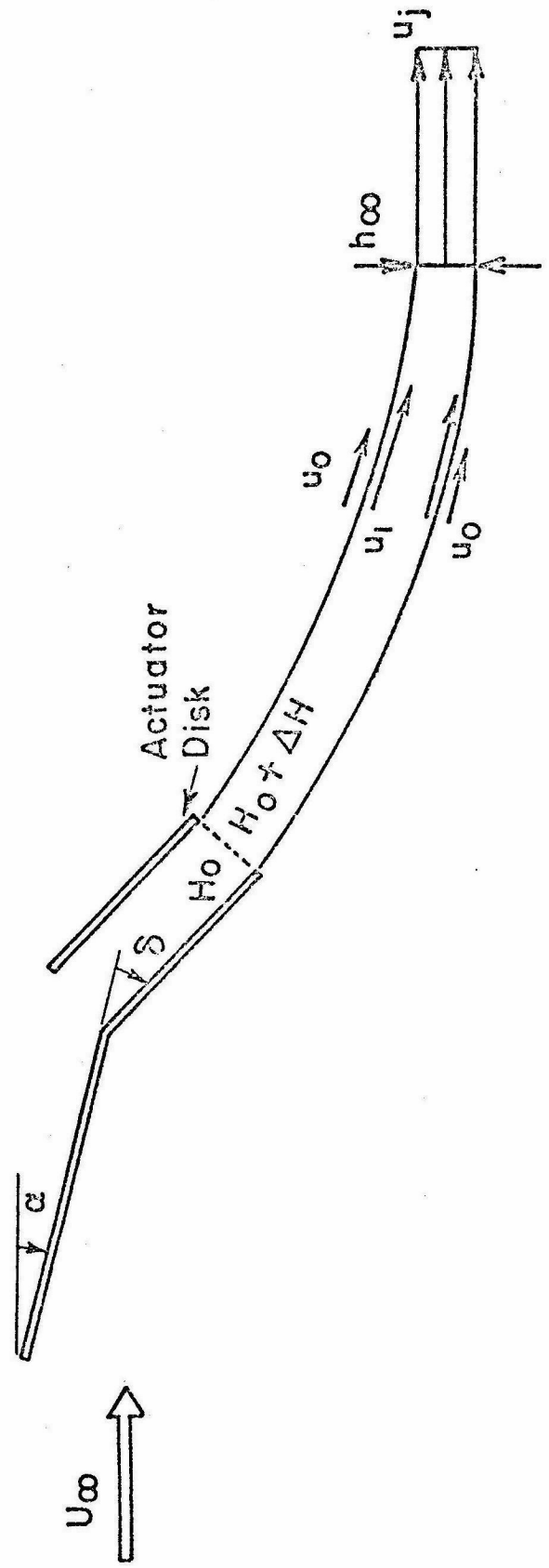

FIG. 2 POTENTIAL FLOW PROBLEM: BASIC GEOMETRY

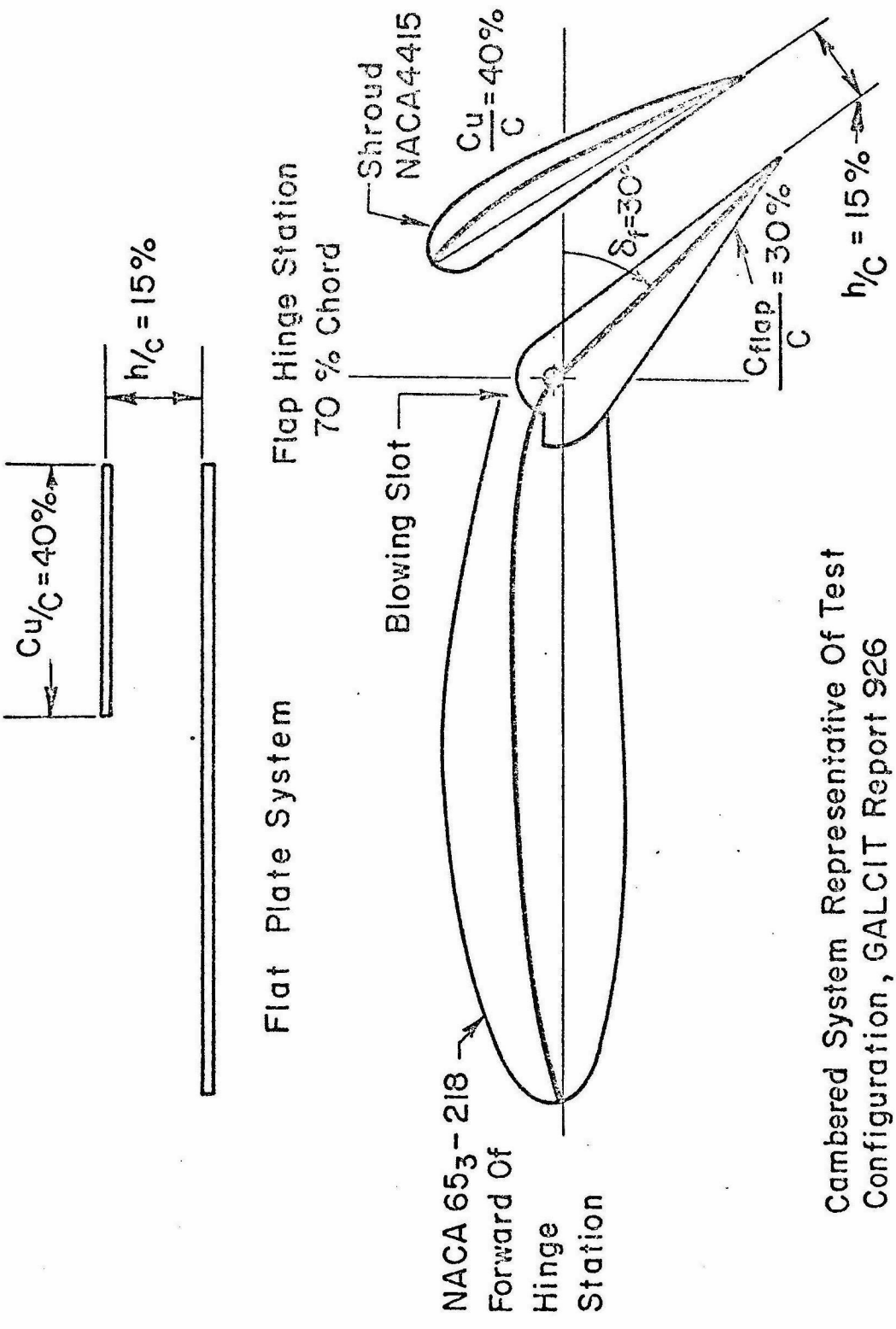

FIG. 2-a SPECIFIC GEOMETRIES USED IN SECTION III

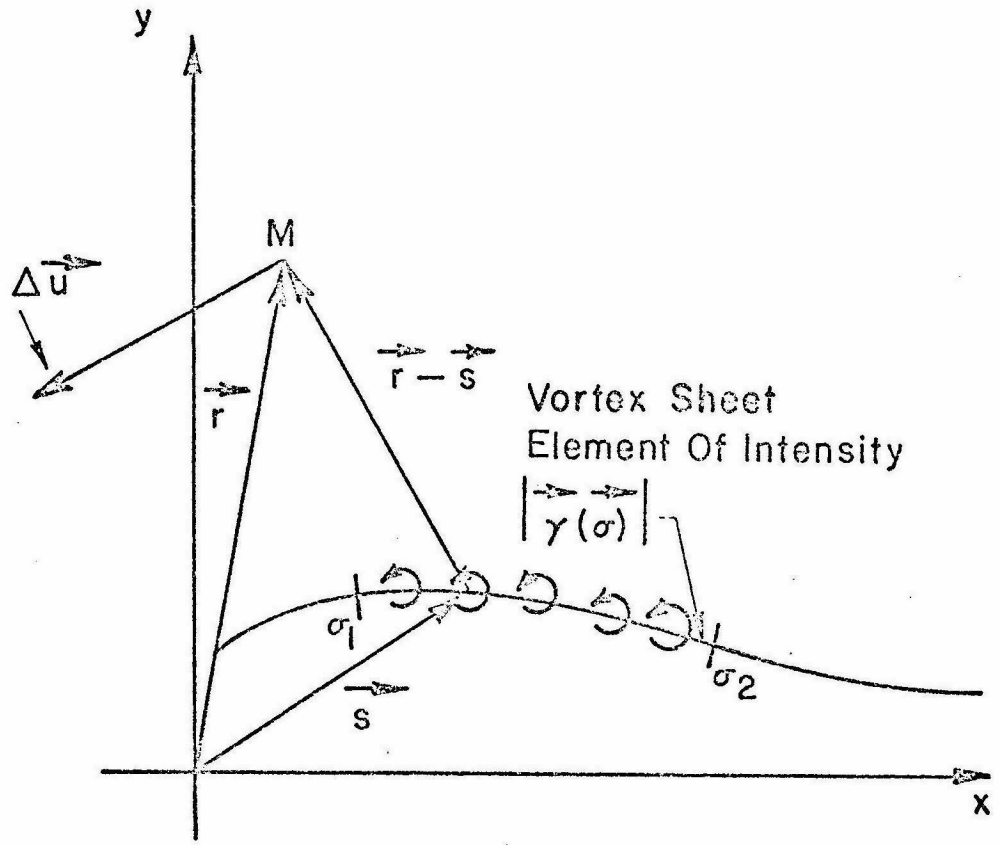

FIG. 3 POISSON SOLUTION TO $\nabla^2 \underline{u} = 0$

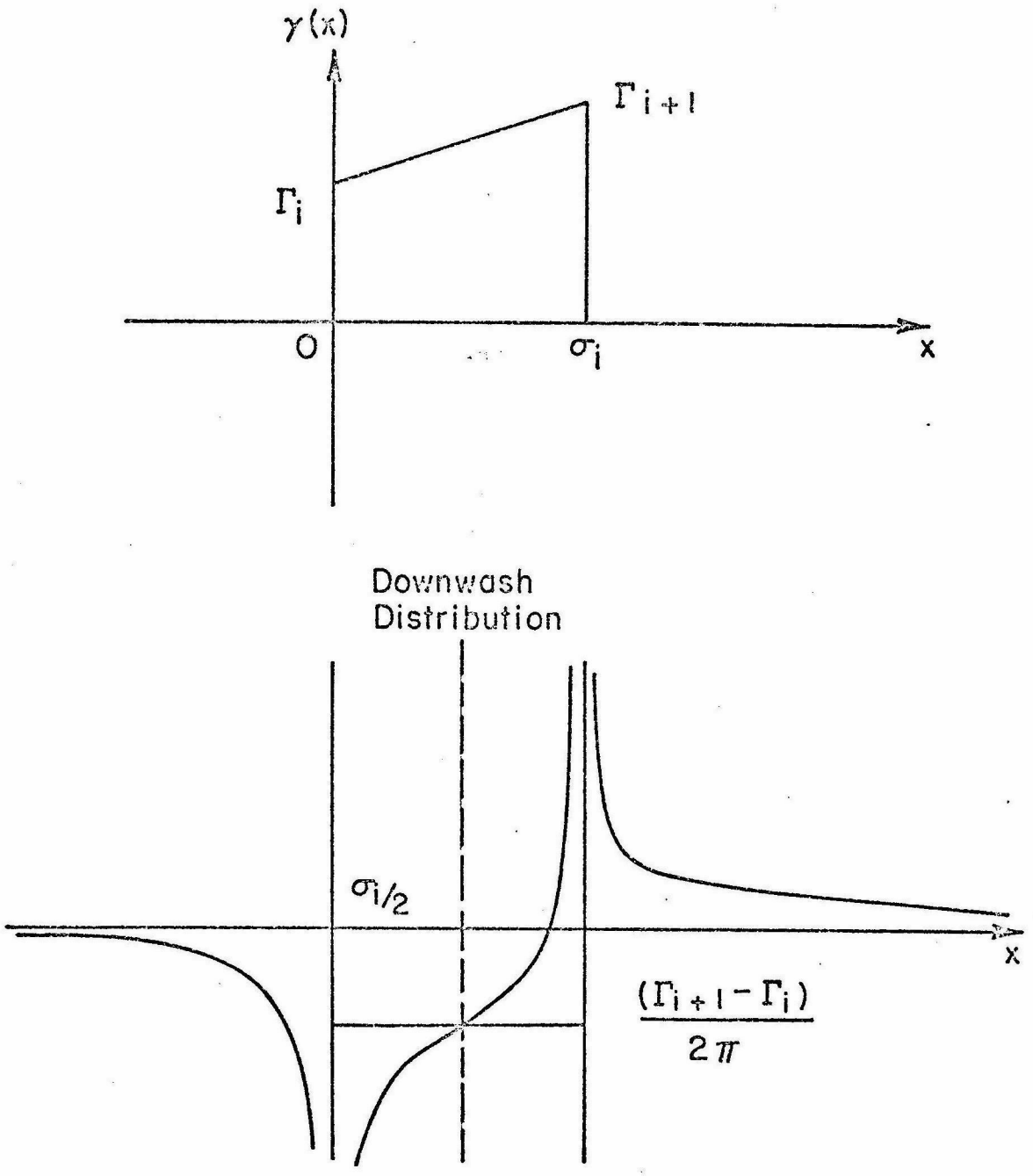

FIG. 4 DOWNWASH OF THE TRAPEZOIDAL VORTICITY

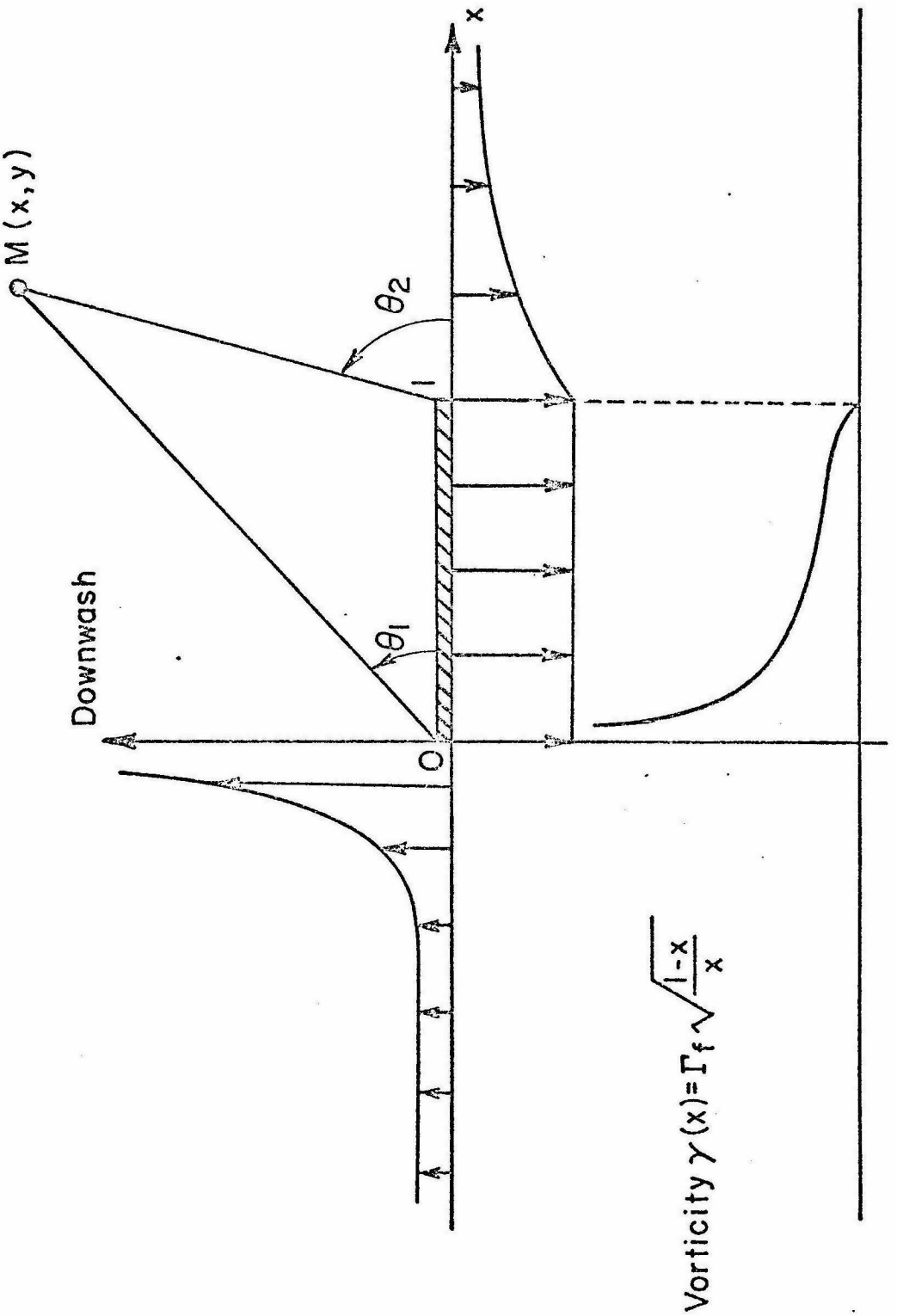

FIG. 5 DOWNWASH FIELD OF NOSE SINGULARITY

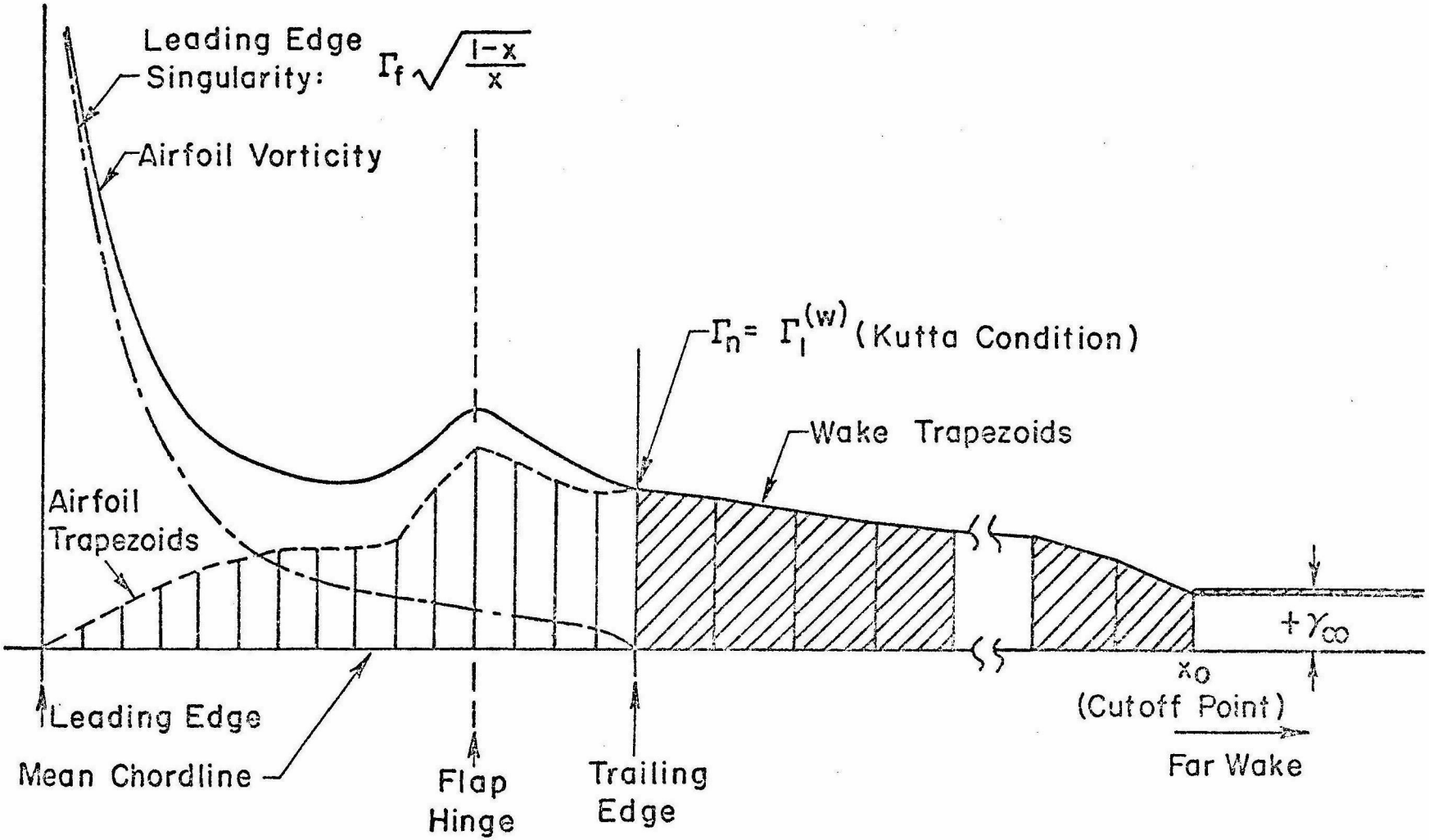

FIG. 6 NUMERICAL REPRESENTATION OF THE VORTICITY (LOWER AIRFOIL)

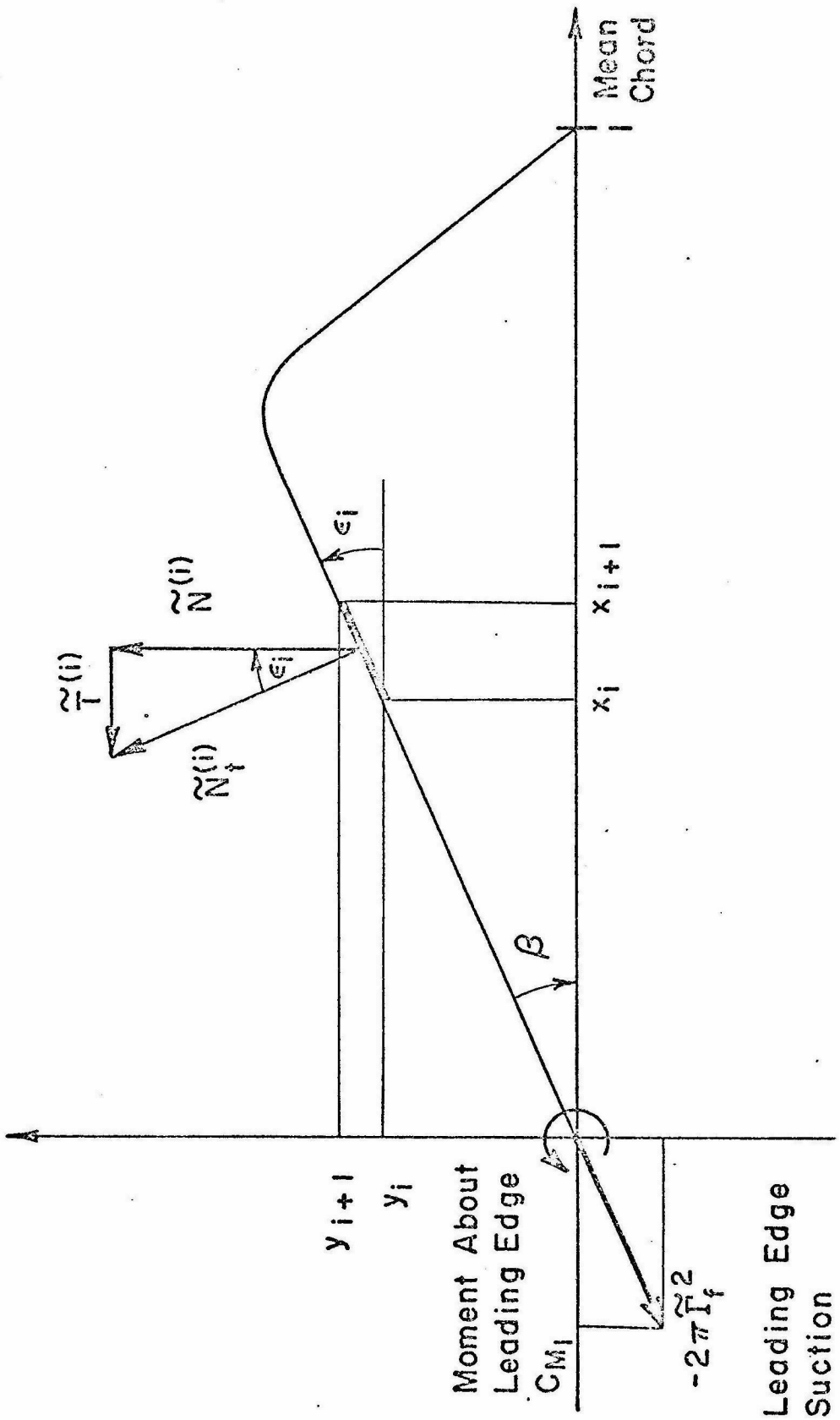

FIG. 7 FORCES/MOMENTS ACTING ON MAIN AIRFOIL

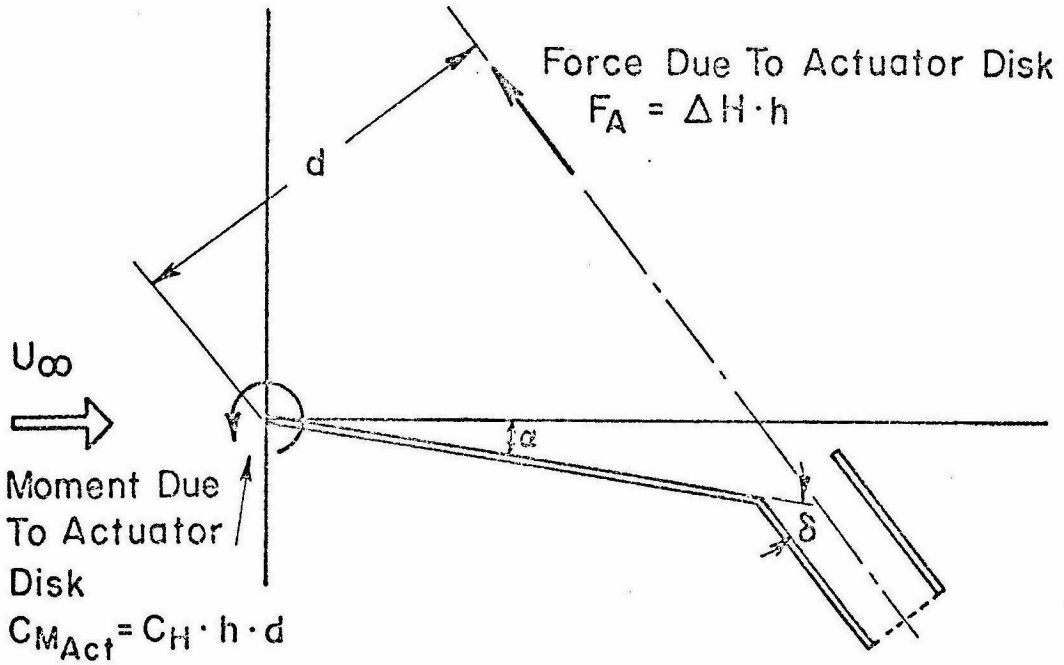

(a) Force And Moment System Due To Actuator Disk

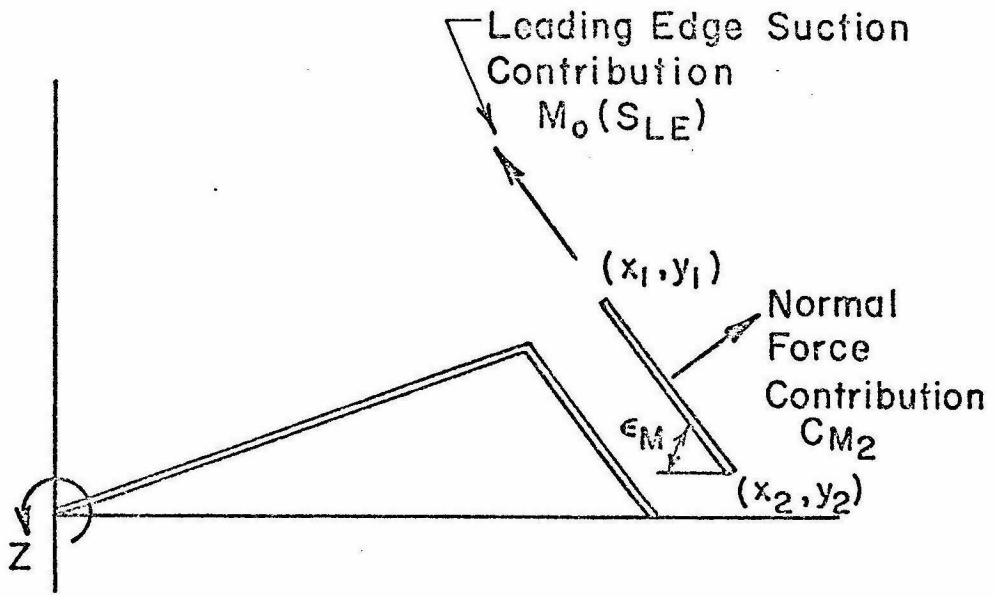

(b) Moment System Due To Upper Airfoil

FIG. 8

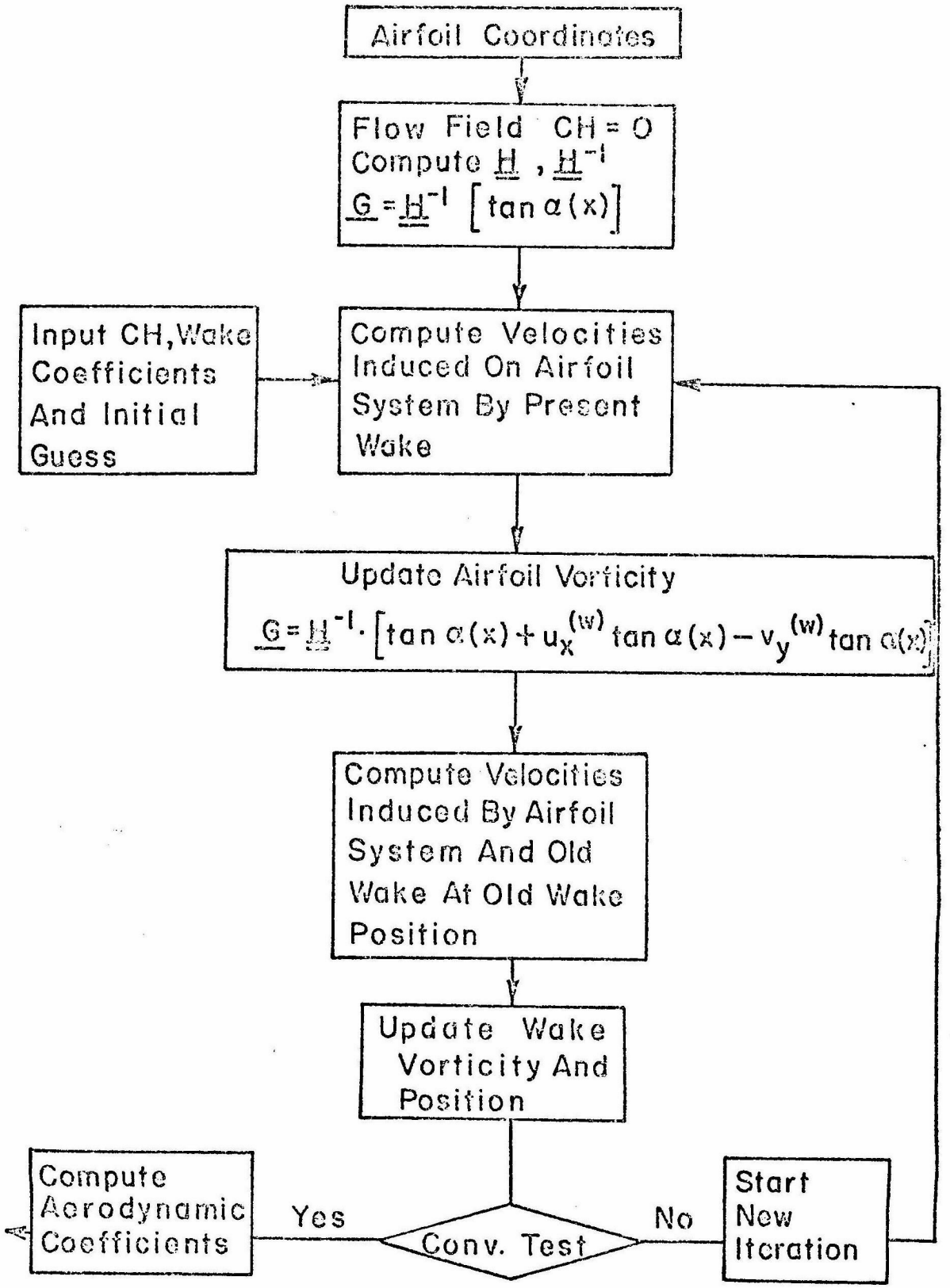

FIG. 9 POTENTIAL FLOW PROGRAM FLOW CHART

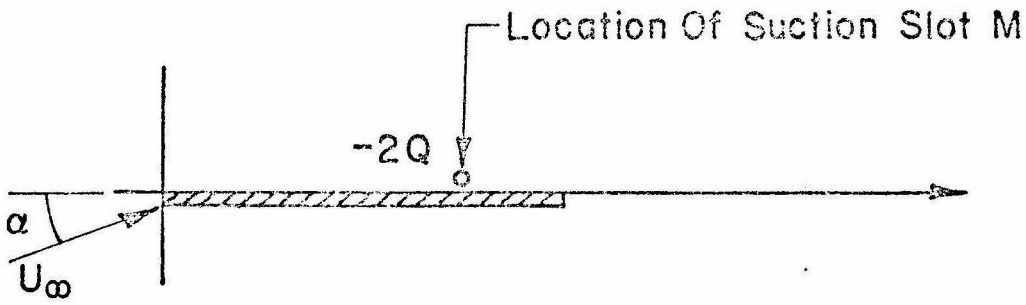

FLAT PLATE AIRFOIL WITH SUCTION SLOT

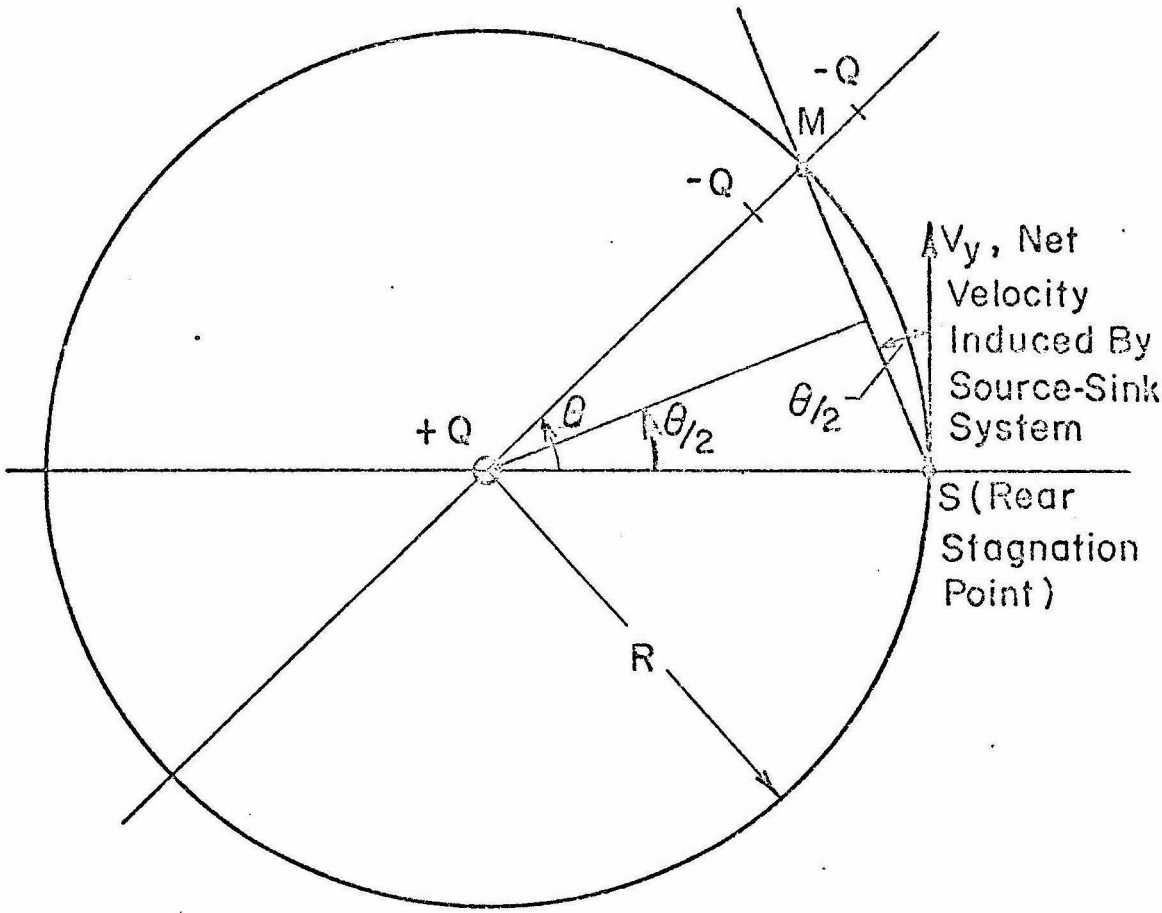

TRANSFORMED FLAT PLATE
AND SINK-SOURCE SYSTEM

FIG. 10 EFFECT OF A SINK ON A FLAT PLATE AIRFOIL

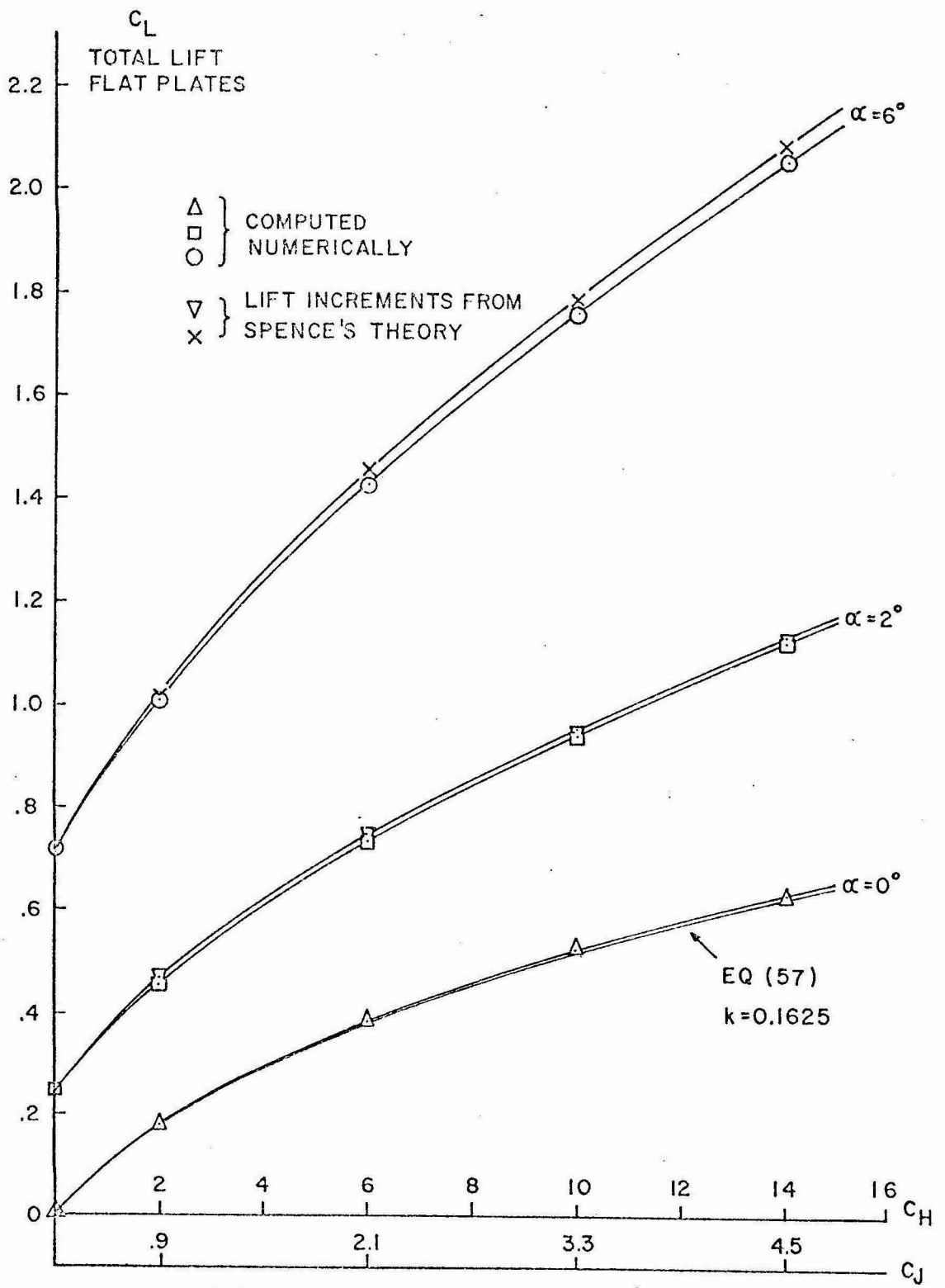

TOTAL LIFT, FLAT PLATE SYSTEM ($^h/_c$ = 15 %)

FIG. 11

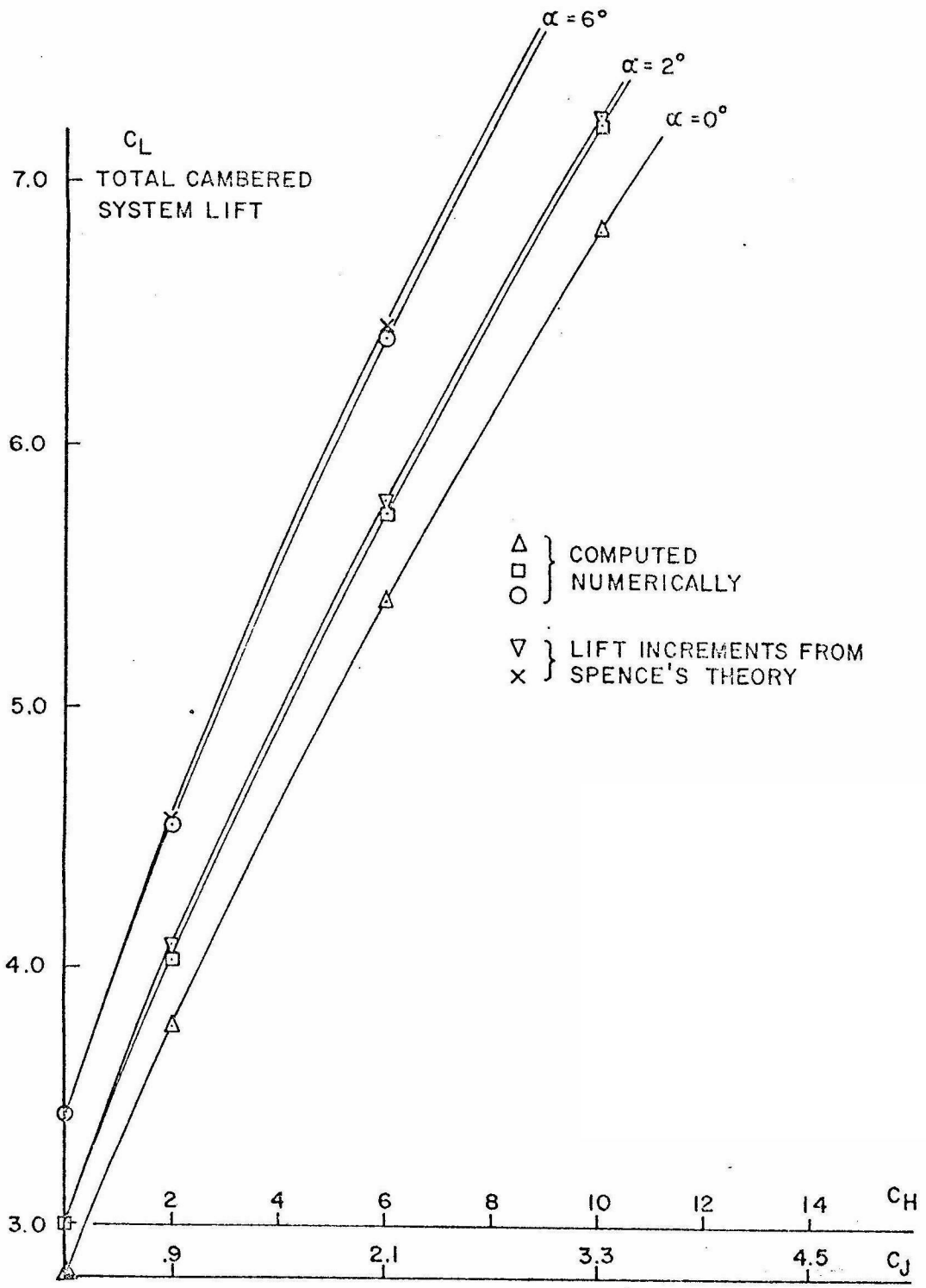

TOTAL LIFT, CAMBERED SYSTEM ($^h/_c$=15%)

FIG. 12

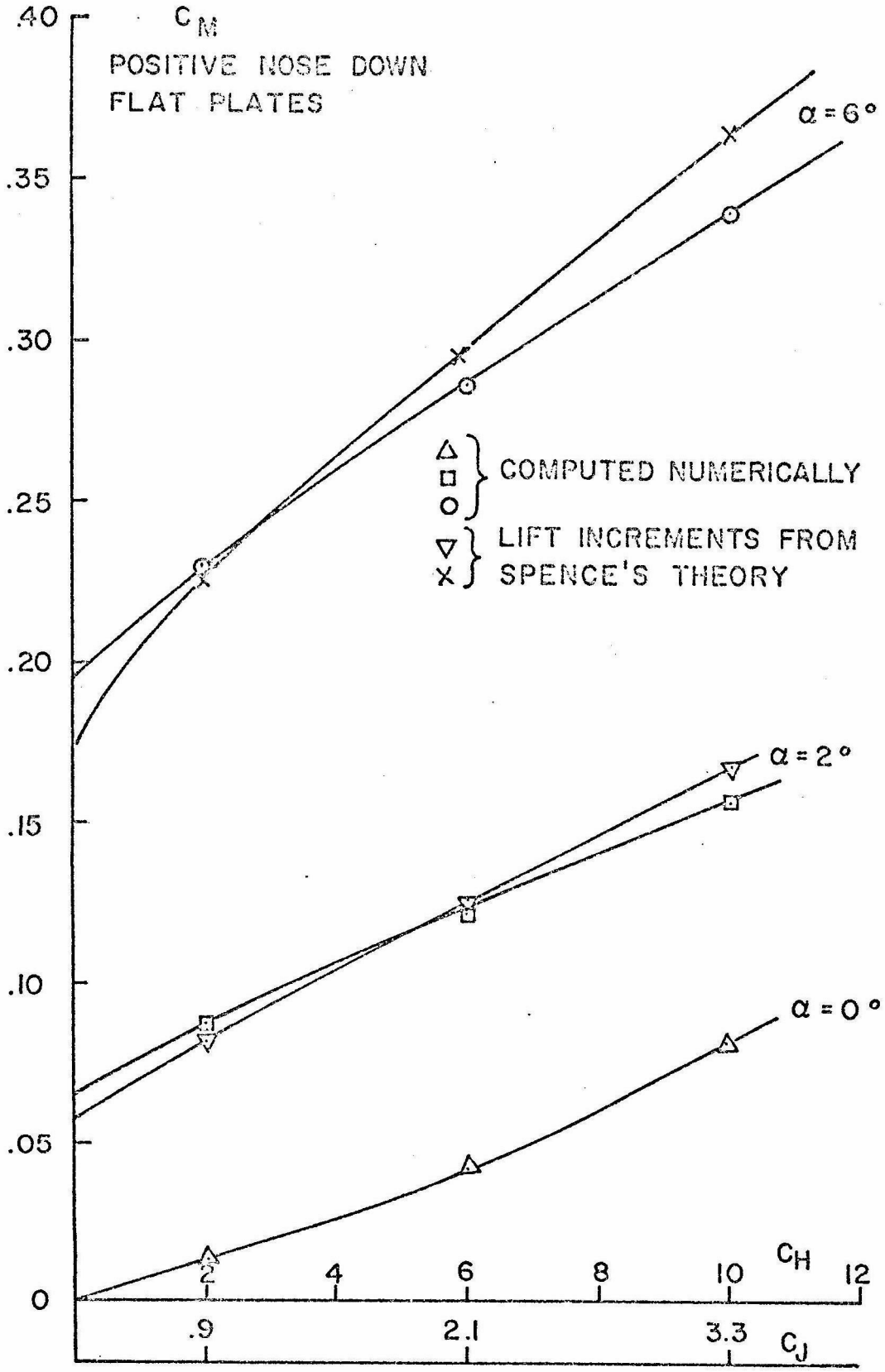

TOTAL MOMENT, FLAT PLATES
FIG. 13

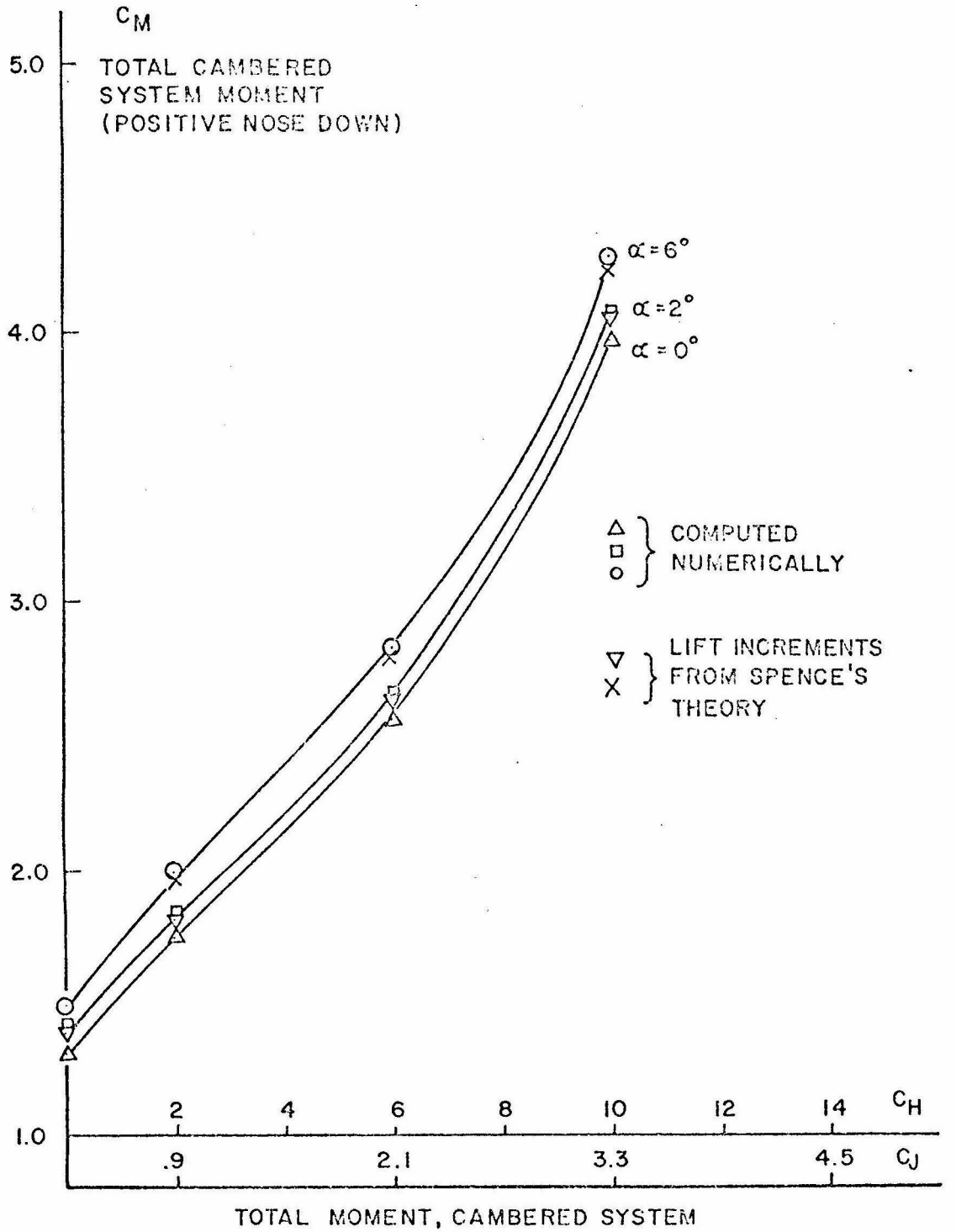
C_M
5.0
TOTAL CAMBERED
SYSTEM MOMENT
(POSITIVE NOSE DOWN)
4.0
3.0
2.0
1.0
α=6°
α=2°
α=0°
COMPUTED
NUMERICALLY
LIFT INCREMENTS
FROM SPENCE'S
THEORY
2
4
6
8
10
12
14
C_H
.9
2.1
3.3
4.5
C_J
TOTAL MOMENT, CAMBERED SYSTEM

FIG. 14

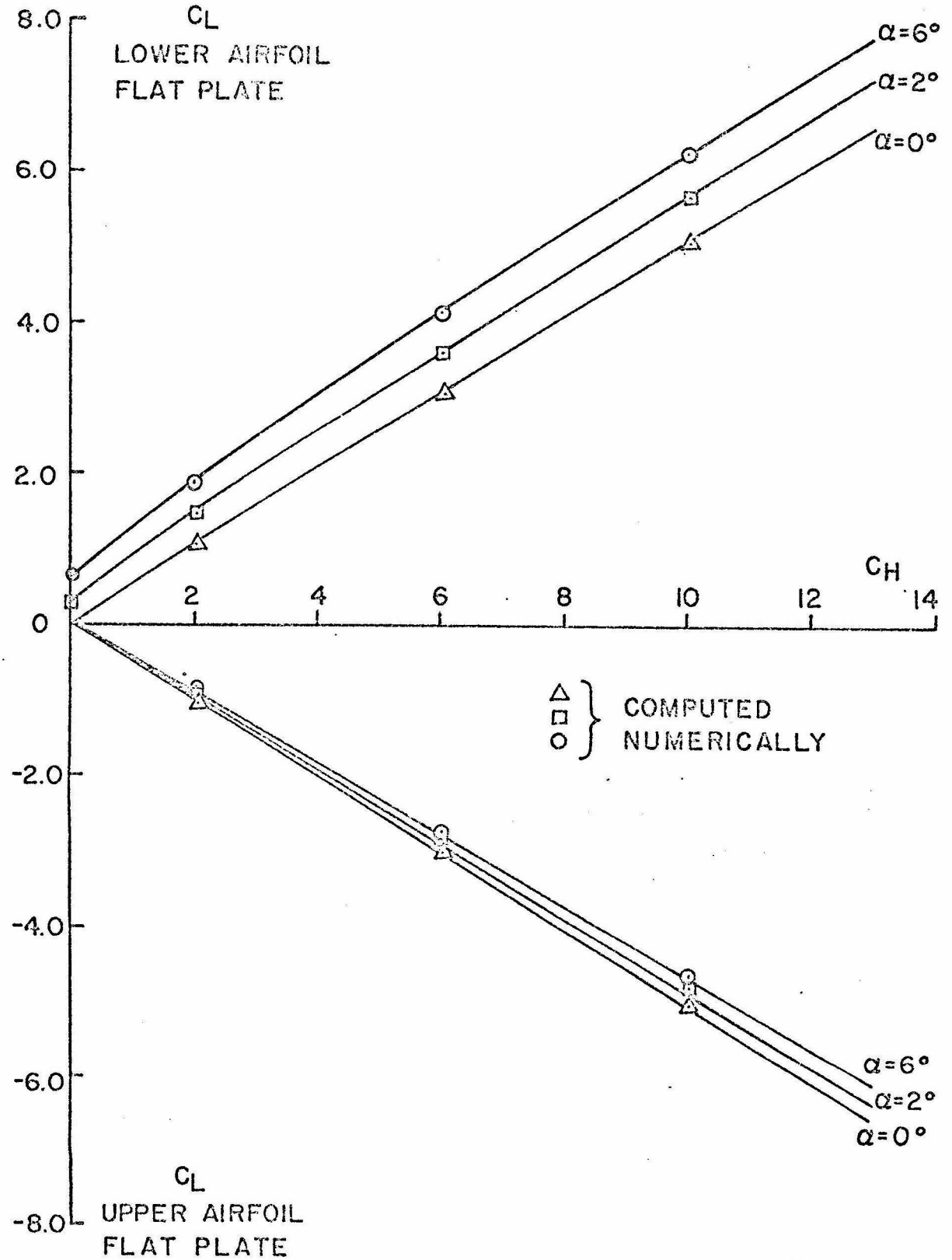

LIFT DISTRIBUTION, FLAT PLATES (ACTUATOR DISK AT TRAILING EDGE

FIG. 15.

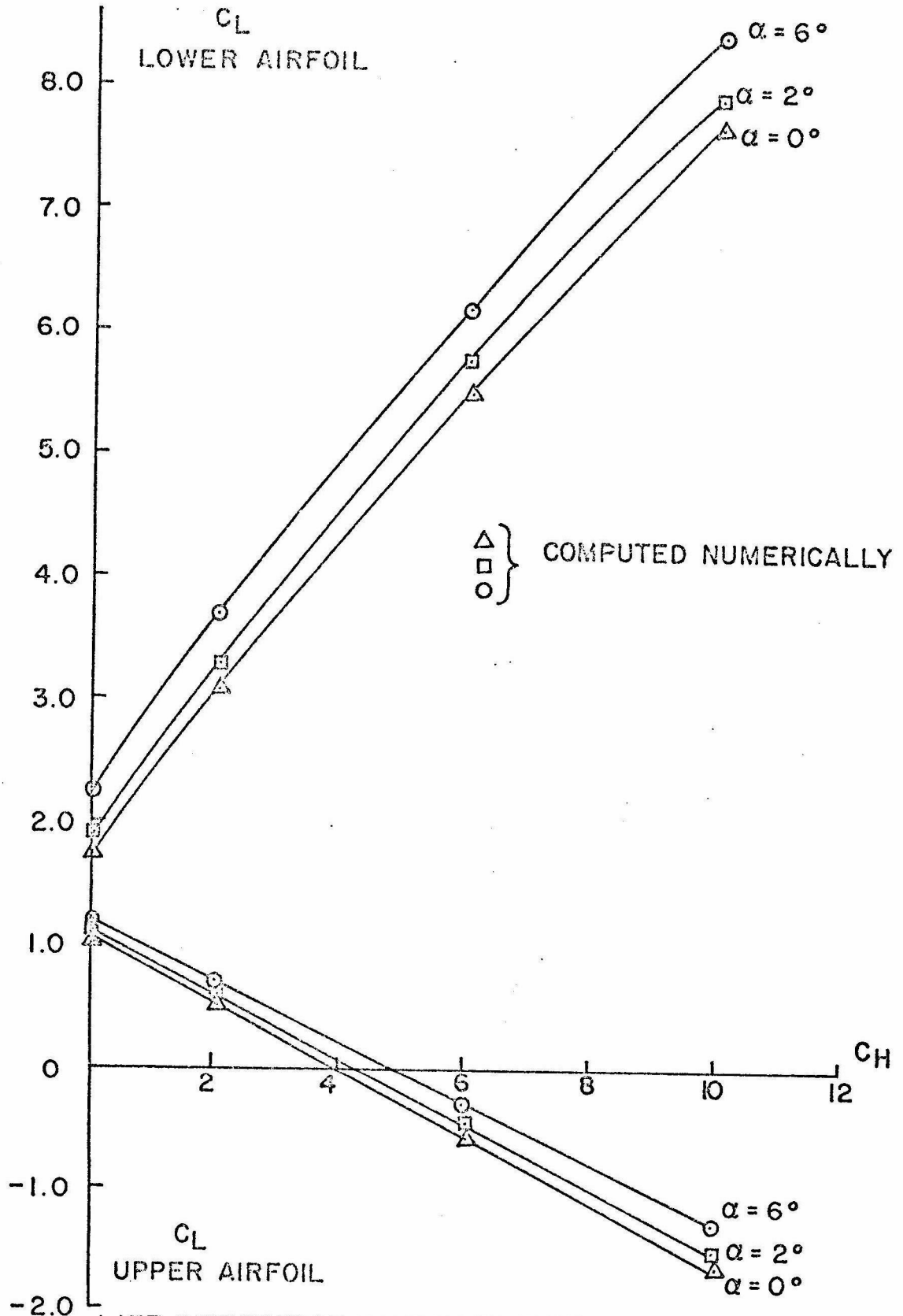

LIFT DISRIBUTION, CAMBERED SYSTEM ACTUATOR DISK AT TRAILING EDGE

FIG. 16